

March 2019

String Out and Compressibility Effect on Pressure Rise in a Shut-In Well

Nicholas Henry

Follow this and additional works at: https://digitalcommons.lsu.edu/gradschool_theses



Part of the [Petroleum Engineering Commons](#)

Recommended Citation

Henry, Nicholas, "String Out and Compressibility Effect on Pressure Rise in a Shut-In Well" (2019). *LSU Master's Theses*. 4862.

https://digitalcommons.lsu.edu/gradschool_theses/4862

This Thesis is brought to you for free and open access by the Graduate School at LSU Digital Commons. It has been accepted for inclusion in LSU Master's Theses by an authorized graduate school editor of LSU Digital Commons. For more information, please contact gradetd@lsu.edu.

STRING OUT AND COMPRESSIBILITY EFFECT ON PRESSURE RISE IN A SHUT-IN WELL

A Thesis

Submitted to the Graduate Faculty of the
Louisiana State University and
Agricultural and Mechanical College
in partial fulfillment of the
requirements for the degree of
Master of Science

in

The Craft & Hawkins Department of Petroleum Engineering

by
Nicholas A. Henry
B.S., University of Houston, 2011
May 2019

Acknowledgements

To Babak Akbari, thank you for all your support, guidance, and challenging discourse throughout this process. To my wife, Laura, you have been my rock and source of refuge. To my committee, Yuanhang Chen and Mayank Tyagi, your guidance has been instrumental. To my colleagues Garrett Nielsen, Jon Estrada, Herman Van Holt, Mahendra Kunju, Dayo Afekare, Muzher Ibrahim, Makuachukwu Mbaegbu, and Roger Hajare.

Table of Contents

Acknowledgements	ii
Nomenclature.....	vii
Abstract.....	viii
Chapter 1. Introduction.....	1
Chapter 2. Literature Review.....	2
Chapter 3. Statement of Problem	18
Chapter 4. Test Matrix.....	19
Chapter 5. Results and Analysis	28
Chapter 6. Case Study	47
Chapter 7. Conclusions	51
Appendix. Experimental Data.....	52
References.....	64
Vita.....	67

List of Tables

Table 1. Table of Inflection Points & Calculated Velocities.....	32
Table 2. Test Liquid Denotations and Properties of Main Experiments	39
Table 3. Fluid Denotations and Rheological Properties of Experiments from Summer 2018	43
Table 4. Summer 2018 Experiments, Average Compressibility Estimates.....	43
Table A.1. Difference in Final Experimental System (Surface) Pressure and Predicted Final System Pressure.....	52
Table A.2. Difference in Pressure Growth Rate due to Bubble Rise	56
Table A.3. Estimate of Liquid Phase Compressibility of Summer 2018 Experiments....	60

List of Figures

Figure 1. Table from Rader et al (1975) Consolidating Significant Previous Results	3
Figure 2. C_1 vs. Bubble Reynold's Number for Griffith & Wallis Correlations	4
Figure 3. C_2 vs. Liquid Reynold's Number for Griffith & Wallis Correlations	4
Figure 4. Chart of Findings by Vianna et al (2003)	9
Figure 5. Pictures of Bubble Formation in Higher Viscosity Liquids	10
Figure 6. Agarwal et al (2007) Derivation of Correlation	12
Figure 7. Agarwal et al (2007) Comparison of Model to Experimental Data	13
Figure 8. Comparison of Bubble Wrap Found in Experiments to Predictions by Image Proplus Software by Agarwal et al (2007) Using Water and Air	14
Figure 9. Axisymmetric Bubble in a Cylindrical Column	16
Figure 10. Main Flow Annulus Schematic (Mohammed Bousaleh)	19
Figure 11. Front View of Experimental Setup	21
Figure 12. Relationship of Apparent Viscosity to Shear Rate Shows a Strong Drop Off as Shear Rate Increases. From Di Giuseppe et al (2014)	27
Figure 13. Pressure vs. Time Graph for a Typical Experiment	28
Figure 14. Section-to-Section Pressure Differentials Used to Find the True Velocity of the Bubble	29
Figure 15. Exhibition of How Bubble Rise Velocity was Found through Time Series Analysis	30
Figure 16. Exhibiting the Difference between a Typical Experiment and the Incompressible and Compressible Models	33
Figure 17. An Example of Gas Kick String Out	34
Figure 18. Known Velocity to Pressure Growth, via Compressible Liquid Model Program Flowchart	36
Figure 19. Known Pressure Growth to Bubble Rise Velocity, via Compressible Liquid Model Program Flowchart	37
Figure 20. Gas Entrainment Precludes the Ability to Analyze the Relationship between Fluid Rheology and Bubble Rise Velocity	39
Figure 21. Measured Final System Pressure vs. Predicted Final System Pressure (+/- 10%)	40

Figure 22. Experimental Pressure Growth Rates against Predicted Pressure Growth Rate Considering Bubble Rise Velocity and Liquid Compressibility.....	41
Figure 23. Difference in Pressure Growth Rate vs. Difference in Final System Pressure	42
Figure 24. Possible, but Very Weak, Correlation between Liquid Yield Stress and Difference between Projected and Actual Final System Pressure	45
Figure 25. Visualization of Gas Kick.....	48
Figure 26. Relationship between Pressure Growth and Liquid Phase Compressibility for a Constant Gas Kick Size and Compressibility	49
Figure 27. Balance Point between System Compressibility and Gas Kick Volume where Gas Bubble Expansion Will Allow Further Influx for a Given Gas Kick Size	50

Nomenclature

Bingham-Plastic Rheological Model. A model of understanding fluid flow behavior in which the material is considered a rigid body at low shear stresses but flows as a viscous fluid at high shear stresses.

Plastic Viscosity. In reference to the Bingham-Plastic Rheological Model, the slope relationship that the shear strain will increase due to increased shear rate.

Rheology. the study of the flow of matter, particularly in a liquid state. Particular interest is given to non-Newtonian, Bingham-Plastic flow behavior in this manuscript.

Yield Stress. In reference to the Bingham-Plastic Rheological Model, the value of shear stress at which the fluid will stop acting as a rigid body and begin to flow.

Abstract

Gas kick migration experiments were performed in a small-scale well prototype model of annular geometry to analyze the behavior of gas kicks in highly non-Newtonian fluids. The objective was to isolate and estimate the effects system compressibility and bubble string out have on the pressure build up in a situation in which a gas kick rises through a noncirculating drilling mud in a vertical well.

The experiments consisted of 2 tests. The first test measured the apparent compressibility of the liquid phase of the experiment – that phase which simulated the drilling mud in a gas kick situation. The second test, performed immediately after the first, was the gas kick test which monitored the pressure rise in a closed-in system in which a gas kick rises through a stagnant liquid phase.

The first test was needed to establish a measure of the compressibility of the liquid phase. Compressibility works to depress the maximum pressure to which a closed system will grow as well as the rate at which the pressure increases. Bubble string out further depresses pressure growth as gas mass is left along the column of liquid. Non-Newtonian rheology increases the likelihood that gas will be entrained by the liquid phase if the liquid exhibits a yield stress.

During the gas kick tests, because the experimental setup was made of steel pipe with no visual confirmation of system dynamics, pressure buildup was monitored at 5 locations – separated by a standard vertical distance for density purposes – throughout the experimental setup. Multiple analyses were made possible by the individual pressure transducers and their relation to each other. Through these analyses, comparisons of the actual bubble rise velocity and the estimate of bubble rise velocity that was made by estimating incompressible liquid phase were able to be compared.

Practical applications of these results include: (1) evidence that the common approach of assuming incompressible liquid phase yields inaccurate results as liquid compressibility increases; (2) a base level of data and evidence needed to establish a link between bubble string out to fluid rheology.

Chapter 1. Introduction

When drilling for oil or natural gas, a catastrophic loss of control over the reservoir fluids can develop, allowing a direct and uncontrollable flow path from reservoir to surface; this major hazard is called a blowout. Blowouts stem from a hazard called a kick. A kick occurs when the drilling fluid exerts less pressure on a permeable reservoir than that reservoir's fluids are under prior to drilling into that section of rock; fluids will flow from areas of higher pressure to areas of lower pressure. If the influx from this initial inflow event is not recognized and dealt with, the (usually) lower density of the influx fluid – relative to the drilling mud – will cause further fluid influx. Gas kicks multiply the level of risk because of gas's tendency to expand when the surrounding pressure decreases and because they tend to rise through the surrounding fluid. For this reason, kicks must be dealt with as soon as possible to keep full control of the wellbore and to exert proper pressure on permeable formations.

Gas bubbles tend to rise through liquids; this phenomenon has been studied experimentally both in situations where liquid is flowing upward and where fluid is stagnant. The gas migration rate needs to be investigated in non-Newtonian fluids enclosed in a pressurized chamber; much like the situation in which a gas kick has entered the well, a kick has been recognized, and the kick has been closed in; decisions can be made once the well is under control, but the gas bubble will continue to migrate. Gas migration in annular geometries can have significant effects on well control and well intervention situations. Common practice is to circulate out the kick as soon as possible to avoid any gas migration or further influx from the reservoir. However, in situations where more advanced methods of well control must be considered and the decision-making process becomes more burdensome, gas migration can become a significant factor in the operating pressure envelope.

Much effort has been given to investigating the migration of gas bubbles while circulating and in stagnant non-Newtonian fluids with no back pressure, but not much attention has been given to how gas bubbles rise in non-Newtonian fluids in an enclosed situation. Compressibility and string out effects affect the ability of onsite personnel to diagnose gas kick location and the ability of these non-Newtonian liquids to entrain small gas bubbles further complicate the relationship between surface pressure growth and bubble rise velocity.

Chapter 2. Literature Review

Gas migration and bubble rise velocity has been a topic of investigation since the 1940s. Authors have been publishing findings since that time in effort to refine the models used to understand bubble rise. This literature review will focus on the development of the bubble rise velocity models for water and other low viscosity Newtonian fluids, the effect that viscosity and geometry have on these models and the expansion of these models into non-Newtonian fluids.

2.1. Early developments with water

Due to their ease and abundance, early investigations – and many modern investigations, for that matter – focus on the behavior of air bubbles in Newtonian fluids such as water and Nitrobenzene. Many of these models focus on tubular geometries as the basis for their formulation, but also find validity in annular geometries. Though not directly applicable to all wellbore environments, these air-Newtonian fluid investigations provide a base of knowledge which can be applied to non-Newtonian fluids and more complex geometries.

Taylor and Davies (1950) were not the first to investigate the migration of bubbles in liquid, but their interest extended into the migration velocity of large bubbles such as those created when submarines are destroyed. Using a revolving drum camera and spark timing, they found that large bubbles rising in extended liquids had a lenticular shape, rounded on the top and relatively flat on the bottom; these types of large, coalesced bubbles have become known as “Taylor Bubbles”. By assuming that the pressure is uniform in the bubble (thus, uniform across the semi-spherical top of the bubble) and similar to an ideal hydrodynamic flow around a complete sphere, Davies and Taylor predicted that the bubble velocity, v_B , through an extended liquid should be related to the radius of curvature of the semi-spherical cap, r_c , and the acceleration of gravity, g , by the following equation.

$$v_B = 0.19\sqrt{gr_c} \quad [1]$$

Very good agreement was found between this equation and their experimental results.

Dumitrescu (1943) examined the behavior of “infinitely long” bubbles migrating through constant diameter tubes. He theoretically computed the approximate shape of a bubble rising in a vertical tube which resulted in a computed profile of rounded nose that resembled a bullet – similar to the profile found in the photos of the Taylor Bubble. By ignoring capillary and frictional effects and considering only the potential and kinetic energy of the liquid flowing past the bubble, the approximate solution for the flow around the front of the bubble was determined by both Dumitrescu and Davies and Taylor. The solution published by Dumitrescu relates bubble velocity, v_B , through a liquid in a vertical tube to the radius of the tube, r_t , and the acceleration due to gravity, g , by the following equation.

$$v_B = 0.101\sqrt{2gr_t} \quad [2]$$

This equation generally agreed with the solution published by Taylor and Davies, which included a constant of 0.134 (which is $0.19/\sqrt{2}$) instead of 0.101; Rader, Bourgoyne, and Ward (1975) consolidated results of several investigators and showed that the results more favorably match Dumitrescu's equation using air and water than Taylor and Davies in larger diameters.

TABLE 1—VELOCITY OF AIR BUBBLES RISING THROUGH WATER IN VERTICAL TUBES

Author	Tube Radius (in.)	Water Viscosity (cp)	Liquid Velocity (ft/sec)	Bubble-Rise* Velocity (ft/sec)	$\frac{v_B}{\sqrt{2gr_t}}$
Davies and Taylor	0.24	1.0	0	0.325	0.083
	0.43	1.0	0	0.490	0.095
	1.56	1.0	0	0.975	0.098
Laird and Chisholm	1.0	1.0	0	0.825	0.103
Griffith and Wallis	0.25	1.3	0	0.35	0.088
			0.39 up	0.43	0.108
			0.81 up	0.50	0.125
	0.38	1.3	0	0.48	0.097
			0.35 up	0.64	0.129
			0.92 up	0.75	0.152
			0.20 down	0.40	0.081
			0	0.58	0.103
	0.50	1.3	0	0.58	0.103
		0.6	0	0.58	0.103
		1.3	0.50 up	0.71	0.126
		1.3	0.99 up	0.81	0.143
		1.3	0.14 down	0.55	0.097
		1.3	0	0.19	0.058
Ward	0.17	1.0	0	0.19	0.058
	2.78	1.0	0	1.41	0.106
	5.00	1.0	0	1.91	0.107

*Relative to liquid velocity

Figure 1. Table from Rader et al (1975) Consolidating Significant Previous Results.

Laird and Chisolm (1956) also investigated bubble rise velocity through water in vertical tubes. They worked with a 2" diameter tube and found bubble rise velocities similar to Davies and Taylor's. But they reported a 10 percent increase in velocity as the length of the bubble was increased from 2 to 25 diameters. However, neither Dumitrescu nor Davies and Taylor included bubble length as a variable in their equations.

Griffith and Wallis (1961) built three 18-ft tubular models with diameters of 0.5, 0.75, and 1.0 in, respectively. They measured bubble-rise velocities in stagnant and moving water. They found that the bubble rise velocity relative to water velocity changed as the water velocity changed. However, contrary to Laird and Chisolm, they found that bubble rise velocity was independent of bubble length once the bubble was long enough to assume a bullet shape; regarding how long it would take for the flow to fully develop, the authors said, "In the 1-in. pipe it was possible to observe bubbles of approximately the ideal form which were 6 ft and more in length". Their findings led to an adjustment of Dumitrescu and Taylor & Davies' original equations to the form:

$$v_B = C_1 C_2 \sqrt{2gr_t} \quad [3]$$

Where C_1 was related to the Bubble Reynolds Number and C_2 was empirically related to the liquid Reynolds Number.

$$N_{RB} = \frac{928\rho_L v_B d}{\mu_L} \quad [4]$$

Regarding Equation 4, N_{rb} refers to the Bubble Reynolds Number. “d” is the diameter of the pipe, assumed to characterize the bubble diameter.

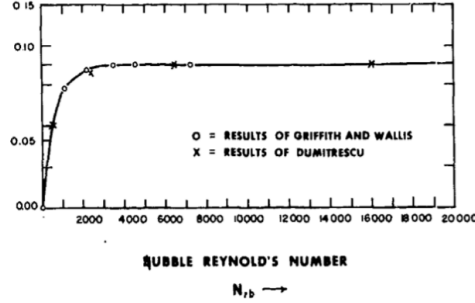


Figure 2. C_1 vs. Bubble Reynolds Number for Griffith & Wallis Correlations

$$N_{RL} = \frac{928\rho_L v_L d}{\mu_L} \quad [5]$$

Reynold's Number of the Liquid Phase

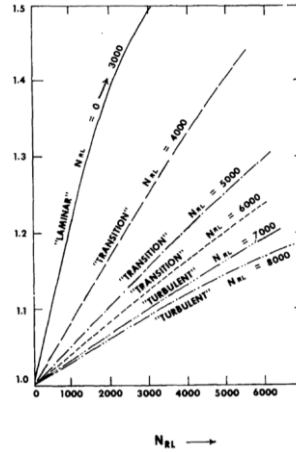


Figure 3. C_2 vs. Liquid Phase Reynold's Number for Griffith & Wallis Correlations

Of interest for its usefulness, Zuber and Findlay (1965) introduced a model by which many subsequent authors analyze their data. This model has particular use for engineering purposes, as will be seen in later engineering studies.

$$V_g = C_0 V_h + V_s \quad [6]$$

where V_g is the mean gas velocity, and V_s is the gas-bubble slip velocity relative to a stationary fluid. The homogeneous velocity, V_h , is defined as

$$V_h = \frac{(Q_g + Q_l)}{A} \quad [7]$$

Where Q_g and Q_l are the volumetric flow rates for the gas and liquid phases, respectively. The coefficient C_0 is related to the distribution of bubbles and their relative velocities across the flow area. If the concentration of gas at the center line of the pipe is smaller than that close to the wall, $C_0 < 1$; in their paper, Zuber & Findlay referenced ‘subcooled boiling’ as an example – where the gas phase evolves along a heater surface without bubble collapse. If the concentration at the center line of the pipe is larger than that at the wall, $C_0 > 1$. In the case of a Taylor Bubble, it is obvious that the concentration along the centerline is higher than that at the wall, thus $C_0 > 1$; Zuber and Findlay observed that C_0 should range between 1.0 and 1.5. This observation was later supported by experimental results.

The results by these subsequent authors, by following the “Taylor Bubble” approach of studying a single coherent bubble in an extended liquid led to closer and closer approximations of Dumitrescu and Taylor & Davies’ initial findings, though most attempted to curve-fit their findings using constants, not always including other parameters, such as viscosity. Length of the bubble is not considered a major influencing factor and the equation is limited to the propagation of a single, large, coherent bubble. However, as the Liquid Reynold’s Number increases, the likelihood that the bubble remaining coherent decreases.

2.2. The Viscous Influence

Because Reynold’s Number has such an effect on the validity of these models, viscosity of the surrounding fluid must affect bubble rise velocity. Generally, given that Reynold’s Number is inversely dependent upon viscosity, an increase in viscosity will lead to a decrease in Reynold’s Number. Many authors have expanded the scope of the early research to include higher viscosity fluids to determine how viscous effects can be modeled into bubble rise velocity.

White & Beardmore (1962) proposed a general graphical correlation for predicting the terminal rise velocity of bubbles in round pipes – the highest achievable velocity of a bubble rising through liquid. They found that the terminal velocity of the bubble was “practically independent of the length of the bubble”, which agreed with previous work.

$$U = \sqrt{gD} \left(\frac{a_1 a_2 \exp(a_3 t)}{a_1 + a_2 (\exp(a_3 t)) - 1} - a_4 \right) \quad [8]$$

where

$$t = \log_{10} \left(\frac{\rho_l g D^2}{\sigma} \right) \quad [9]$$

σ is surface tension of the fluid phase

$$a_i = \sum_{j=1}^8 c_{ij} x^{j-1} \quad (i = 1, 2, 3, 4) \quad [10]$$

$$x = \log_{10} \left(\frac{g \mu^4}{\rho_l \sigma^3} \right) \quad [11]$$

μ is liquid viscosity and coefficients c_{ij} are

$$c_{ij} = \begin{bmatrix} 3.5603852 \times 10^{-1} & 2.6717658 \times 10^{-3} & -2.7121907 \times 10^{-3} & -2.0001955 \times 10^{-3} \\ 1.5642441 \times 10^{-3} & 2.8532721 \times 10^{-4} & -4.7831508 \times 10^{-5} & -3.605927 \times 10^{-5} \\ 3.059819 & -5.2352564 \times 10^{-1} & 3.3906415 \times 10^{-2} & 2.1368428 \times 10^{-2} \dots \\ 2.3221312 \times 10^{-2} & -1.809746 \times 10^{-3} & 9.3468732 \times 10^{-5} & -2.3440168 \times 10^{-4} \end{bmatrix}$$

$$\begin{bmatrix} 8.622533 \times 10^{-5} & 5.7198751 \times 10^{-5} & -2.4316663 \times 10^{-6} & -6.7582431 \times 10^{-7} \\ 7.6382727 \times 10^{-6} & 1.1736259 \times 10^{-6} & -1.5186036 \times 10^{-7} & -1.9756221 \times 10^{-8} \\ \dots & -3.2676237 \times 10^{-3} & -7.302279 \times 10^{-4} & 7.2215493 \times 10^{-5} \\ 5.9716008 \times 10^{-5} & 9.7852173 \times 10^{-6} & -1.3514105 \times 10^{-6} & -1.74642 \times 10^{-7} \end{bmatrix}$$

$\frac{g\mu^4}{\rho_l\sigma^3}$ was referred to by White and Beardmore as property group Y but was later referred to by Cliff *et al.* (1978) as the Morton Number (M).

$$\text{Eötvös Number, } E_o = \frac{g\rho_l D^2}{\sigma} \quad [12]$$

$$5 < E_o < 1000, 10^{-8} < Y < 10^6$$

The White & Beardmore model led to a relatively high squared residuals sum of Froude Number $Fr = \frac{U}{(gD)^{1/2}}$ when tested against the data; representing the departure of the results from the model's predictions. The Froude Number was selected by these investigators to be the sole dimensionless number containing u , the velocity of the bubble.

$$\sum (Fr_{meas} - Fr_{calc})^2 = 0.23$$

Nevertheless, White & Beardmore provided a template for a much more recent correlation.

Goldsmith & Mason (1962) found that for a constant value of E_o , the overall bubble deformation (nose, film, and tail) remained independent of the liquid viscosity. Nicklin, Wilkes, & Davidson (1962) investigated the dependence of rise velocity and bubble length. They accurately predicted the rise velocity of Taylor bubbles; regarding this, they commented that '...this (migration) velocity is independent of the slug length and is modified only by a net flow of liquid across a section above the slug'. They also suggested that: (i) a slug can be broken into sections of a nose where the liquid accelerates under gravity and a lower region in which gravity is balanced by wall shear forces and (ii) slugs generally tend to rise as quickly as possible.

Brown (1965) performed an experimental and theoretical study on the effect of liquid viscosity on the terminal rise of Taylor Bubbles. The solution he found was not suitable for higher viscosity fluids, but of significant value, he found that the noses of different Taylor bubbles exhibited similar geometries, regardless of the fluid viscosity. This agreed with Goldsmith & Mason's findings which led Brown to propose a more general form, including the retarding effect of liquid viscosity.

$$U = 0.35\sqrt{gD} \sqrt{1 - 2\left(\frac{\sqrt{1+ND}-1}{ND}\right)} \quad [13]$$

Where

$$N = \left(14.5 \frac{\rho_l^2 g}{\mu^2}\right)^{1/3} \quad [14]$$

ND is dimensionless

The limits of the applicability of their results were established empirically as

$$\text{Surface Tension: } \frac{\rho_l g D^2}{4\sigma} \left(1 - 2 \left(\frac{\sqrt{1+ND}-1}{ND}\right)\right)^2 > 5.0,$$

$$ND > 60.$$

Zukoski (1966) performed an extensive study of the relevant variables that influence the rise velocity of Taylor bubbles (density, pipe diameter, surface tension, viscosity, and pipe inclination). He took literature data as well as his own and used a set of dimensionless numbers to analyze the data set. Those dimensionless numbers were the Reynold's Number ($R = \frac{\rho_l U D}{2\mu}$), Dimensionless Velocity ($Fr_z = \frac{U}{\sqrt{gD/2}}$), and the

Surface Tension Number ($\Sigma = \frac{4\sigma}{\rho_l g D^2}$); U refers to the rise velocity of the bubble. He found that when Reynold's Number is greater than 200, the rise velocities are "substantially independent" of viscous effects which implies that the bubble's movement is solely controlled by Σ . Also, for $\Sigma < 0.1$, the rise velocity is basically equal to Dumitrescu's modeling equation. The effects of viscosity and surface tension are combined using

$$Fr_z(R_z, \Sigma) = Fr_z(\infty, \Sigma) f(R_z).$$

Fitting to his data, Zukoski shared the following numerical form:

$$Fr_z(\infty, \Sigma) = 0.4664 + 0.3473\Sigma - 5.3928\Sigma^2 + 10.532\Sigma^3 - 6.7095\Sigma^4 \quad (\Sigma < 0.6), \quad [15]$$

$$f(R_z) = \frac{1}{\left(1 + 44.72/R_z^{1.8}\right)^{0.279}}. \quad [16]$$

Thus, from Zukoski's work, given a set of physical properties and pipe radius, the bubble's rise velocity can be calculated through a numerical method using the 3 above equations; $R_z = R * Fr/2$ and $\Sigma = 4/E_o$. The sum of squared residuals for this model is 0.07. As White & Beardmore approached this problem, Zukoski used the Froude Number as the dependent variable and proxy for bubble velocity.

Wallis (1969) proposed a general correlation for Taylor bubble rise velocity in terms of all relevant variables

$$U = k \sqrt{\left(\frac{Dg(\rho_l - \rho_g)}{\rho_l}\right)} \quad [17]$$

and

$$k = 0.345 \left(1 - e^{-0.01R/0.345} \right) \left(1 - e^{(3.37-Eo)/m} \right), \quad [18]$$

R is the buoyancy Reynold's Number:

$$R = \frac{\sqrt{D^3 g (\rho_l - \rho_g) \rho_l}}{\mu}; \quad [19]$$

m is a function of R and takes on the values:

$$\begin{cases} R > 250 & m = 10 \\ 18 < R < 250 & m = 69R^{-0.35} \\ R < 18 & m = 25 \end{cases}$$

The performance of Wallis's correlation fares very well. The sum of the squared residuals is 0.06; this was calculated by the difference in results of Wallis' proposed model and results of 251 experiments; consolidated by Viana *et al* (2003).

Finally, Viana *et al* (2003) performed an extensive literature review of Taylor Bubble methodology and subsequently published findings on a universal correlation of the rise velocity of long gas bubbles in round pipes that resulted in findings that matched their experimental findings closer than any other model previously developed, exhibited by their sum of residual squares. They compared their results to Wallis (1969) and Zukoski (1966), finding that their model exhibited the best overall fit to the data, with a sum of residual squares of 0.03. However, this correlation was much more complicated than the previous Wallis or Zukoski's.

$$Fr = L[R; A, B, C, G] = \frac{A}{\left(1 + \left(\frac{R}{B} \right)^C \right)^G}, \quad [20]$$

where

$$A=L[Eo; a,b,c,d], \quad B=L[Eo; e,f,g,h], \quad C=L[Eo; i,j,k,l], \quad G=m/C,$$

and the parameters (a,b,\dots,l) are:

$$\begin{array}{lllll} a=0.34; & b=14.793; & c=-3.06; & d=0.58; & e=31.08; \\ f=29.868; & g=-1.96; & h=-0.49 & i=-1.45; & j=24.867; \\ & k=-9.93; & l=-0.094; & m=-1.0295. & \end{array}$$

This elaborate function describes all their data with $Eo > 6$.

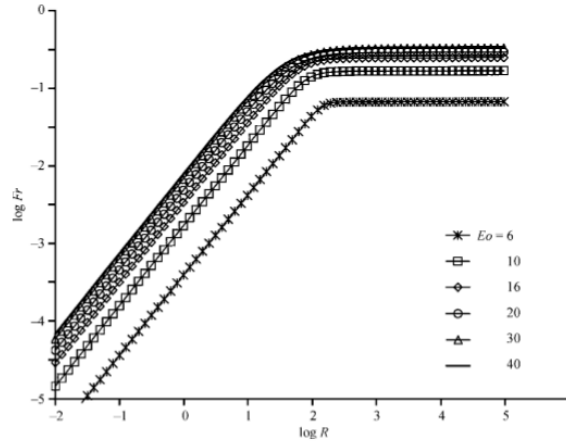


Figure 4. Chart of Findings by Vianna et al (2003)

Important Dimensionless Parameters	Limits	Retarding Forces other than inertia	Equation
Fr	$R > 200$ and $Eo > 40$	None	$Fr = 0.34$
Fr, Eo	$R > 200$ and $6 < Eo < 40$	Interfacial	$Fr = 2.431 \times 10^{-3} Eo^{1.783}$
Fr, R	$R < 10$ and $Eo > 40$	Viscous	$Fr = 9.494 \times 10^{-3} R^{1.026}$
Fr, R, Eo	$R < 10$ and $6 < Eo < 49$	Viscous and interfacial	$\frac{Fr}{R^{1.026}} = 4.417 \times 10^{-5} Eo^{1.484}$
Fr, R, Eo	$Eo > 6$	Viscous and interfacial	See expanded equation and coefficients above

Of further interest, they published pictures of Taylor Bubbles in various viscous fluids:

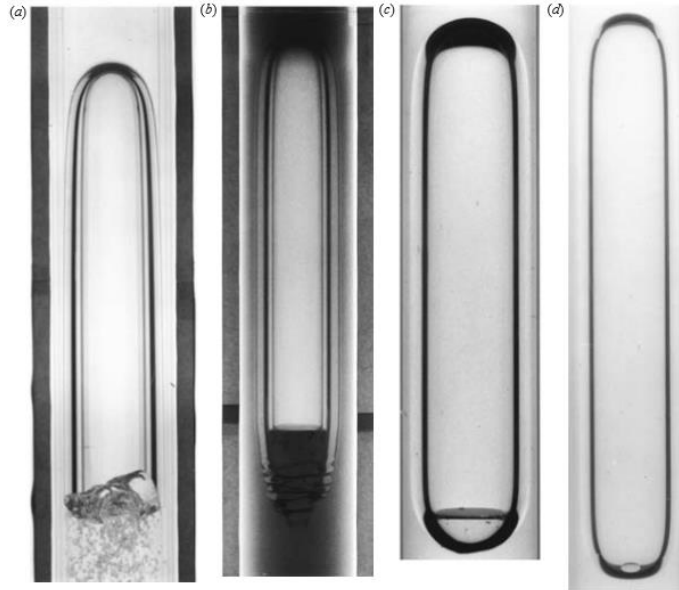


Figure 5. Pictures of Bubble Formation in Higher Viscosity Liquids. Photographs of Taylor Bubbles Rising through 76.2 mm Inside-Diameter Pipe Filled with Different Viscosity Liquids: (a) Water; (b) Purolub 150 Oil (480 mPa s); (c) Silicone Oil (1300 mPa s); Silicone Oil (3900 mPa s). Viana et al (2003)

As can be seen in the above photos from the work done by Viana *et al.* (2003), the “bullet shape” described by Taylor & Davies (1950) and Dumitrescu (1943) can be seen in photo (a); it seems obvious that the viscosity of the surrounding fluid and turbulence created in the thin fluid flow section between the bubble and the wall determine the shape of the tail section.

The extensive work investigating Taylor bubble behavior has led to very precise approximation models of this motion (though, that precision may come at the cost of simplicity); the same cannot quite be said for the effect of introducing an annular geometry.

2.3. Annular Geometry

An annulus is the cylindrical space between two cylinders. It is a very important and common geometry encountered in drilling and well intervention operations. Significantly less investigations have been performed on the effect that annular geometries have on the gas migration phenomena, but it stands to reason that if shear forces play an important part in retarding the flow of a bubble, then the introduction of a second solid face should add to the shear forces along the long portion of the bubble, affecting its ability to move up the annulus.

Rader *et al.* (1975) took Taylor & Davies’ work into consideration and expanded the investigation into annular geometries. They found that both bubble rise velocity and bubble fragmentation significantly affect the annular pressures encountered during well control operations. They found that a gas bubble rising in a vertical annulus will travel up one side of the annulus with liquid backflow occupying the area opposite the bubble.

They also found, for their investigation, that length of the bubble, surface tension between the gas and liquid, and eccentricity of the annulus had little effect on the rise velocity of a single continuous bubble. They found that the correlations proposed by previous studies could be successfully modified for annular geometries, but those modified correlations were inapplicable to their large-scale field tests where bubble fragmentation was a significant factor. They proposed a modified version of Griffith & Wallis' equation, which was a modification of Davies & Taylor's equation, as such:

$$U = 10C_1\sqrt{F_g}C_2C_3\sqrt{\frac{(r_{c1}+r_{c2})(\rho_L-\rho_G)}{\rho_L}} \quad [21]$$

where r_{c1} and r_{c2} are the major and minor radii of curvature of the elliptic cap of the Taylor bubble, C_1F_g accounts for the effect of viscous characteristics of the liquid; F_g is gravitational force, C_3 accounts for the effect of bubble expansion on the velocity, ρ_L is the density of liquid and ρ_G is the density of gas.

In a particularly relevant investigation into gas rise velocities from full scale kick experiments, Hovland and Rommetveit (1992) analyzed 24 full scale gas kick experiments performed in a 2020m long research well. They found, in context of analyzing the free gas front of the gas kick by the Zuber-Findlay model, $C_0=0.72$ (distribution coefficient) and a $V_s=0.27$ for high void fraction and $V_s=0.19$ in low and medium void fraction, both in Water Based Mud. They commented that the free gas front velocity, the tip of the Taylor Bubble, had not been found to be significantly dependent upon the gas void fraction, well inclination, mud density, viscosity, nor surface tension.

Making use of the extensive previous work discussed in Section 2.2, Das *et al.* (1998) took literature data as well as their own to find a model of the rise velocity of a Taylor bubble in a concentric annulus. They comment on previous annuli and round pipe literature that the closest approximation to predicting gas rise velocity came from an approach of applying Froude Number, K , to an equation in the form of Taylor & Davies:

$$U = K\sqrt{gD^*} \quad [22]$$

Where D^* is the characteristic dimension. They correctly point out that many previous authors had put forth definitions of D^* that “were entirely arbitrary and had no physical basis.” They eliminated the elaborate constructions of D^* and found good agreement with their model

$$U = 0.323\sqrt{g(D_1 + D_2)} \quad [23]$$

The characteristic dimension was found to be (D_1+D_2) which is different from the hydraulic diameter (D_1-D_2) . They comment on the shortcomings of this model, stating “extensive experimentations are required to verify the shape of the bubble cap and the liquid velocity profile.” Finally, they observed that Taylor bubbles rise faster in annuli than in round pipes, given the same diameter of the outside bound.

Das *et al.* (2002) followed upon their previous work, to provide further investigation into the geometry that Taylor bubbles take in annuli. Both investigations

found that the bubble will wrap almost completely around the inner pipe, but not completely – leaving a liquid bridge or gap. Das *et al.* found a linear relationship between volume and length of the bubble, above a small nonlinear section – likely at the point below which gas does not fill the annular cross section. Given the importance that has been placed upon the ellipsoidal radii of the nose section of Taylor bubbles, the findings of Das *et al.* give a template on realistic bubble shapes given the annular geometry and bubble volume.

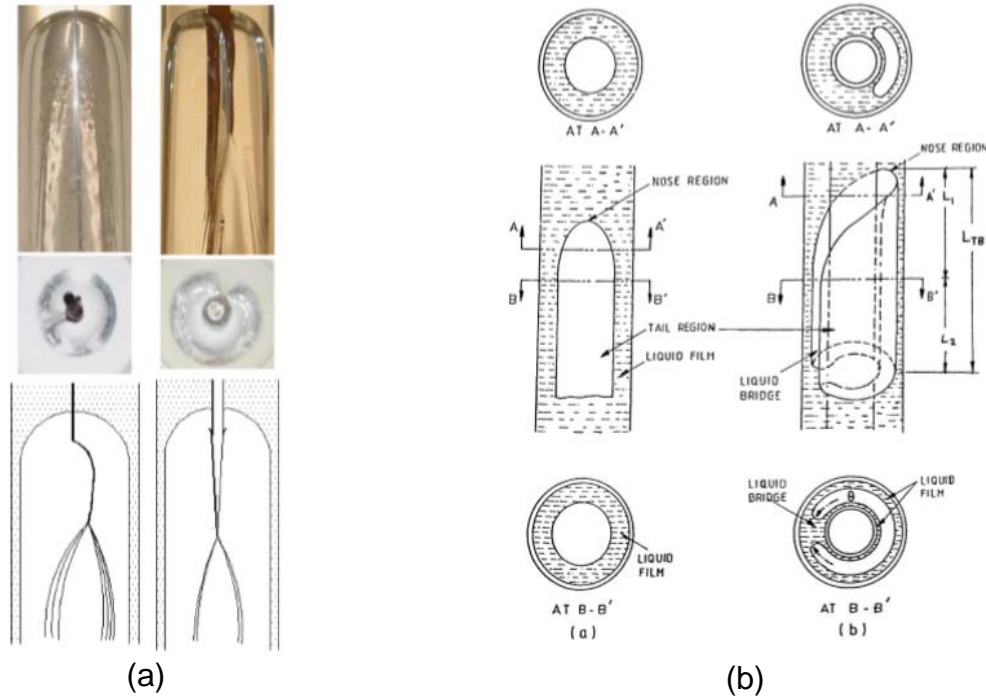
Agarwal *et al* (2007) followed up further on the work performed by Das *et al.* (2002). They comment, “it is established that the rise velocity of an elongated bubble depends on the shape of its nose. The Taylor bubble rising through a circular annulus bears a striking similarity to an elliptic cap bubble rising through parallel plates.” Using the previously discussed equation $U_{TB} = Fr \sqrt{2gp}$ where U_{TB} , p , and Fr are the rise velocity of the Taylor bubble, the wetted perimeter, and Froude Number, respectively, they found a very good approximation of Taylor bubble rise velocity. Within the context of concentric circular annuli, the equation can be reduced to:

$$U = \frac{b}{a+b} \sqrt{ga} \quad [24]$$

where a and b are the semi-major and semi-minor axes of the bubble,

$$b = p\theta,$$

$$a/b = \frac{1}{(1-\theta)^2},$$



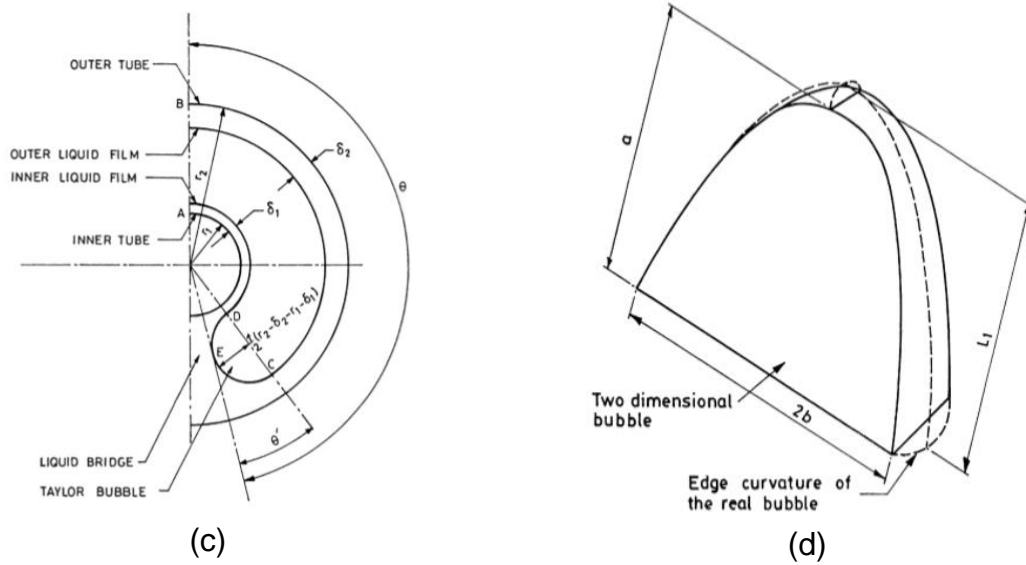


Figure 6. Agarwal et al (2007) Derivation of Correlation.

- (a) Pictures of bubble wrap around inner pipe of annulus. Introduction of the idea that as the inner pipe decreases to a very thin pipe, the bubble continues its 'wrap' geometry. Das et al (2002)
- (b) Characterization of annular bubble. Broken into nose and body sections. Agarwal et al (2007)
- (c) Top-down view of bubble. Description of Wrap Angle, θ . Agarwal et al (2007)
- (d) Description of Nose Section of bubble. Semi-major (a) and semi-minor (b) axes of bubble for use in equation [24]. Agarwal et al (2007)

where θ is the angle of wrap of the bubbles. When reduced to this form, a very good approximation of the bubble rise velocity is found; results are shown below:

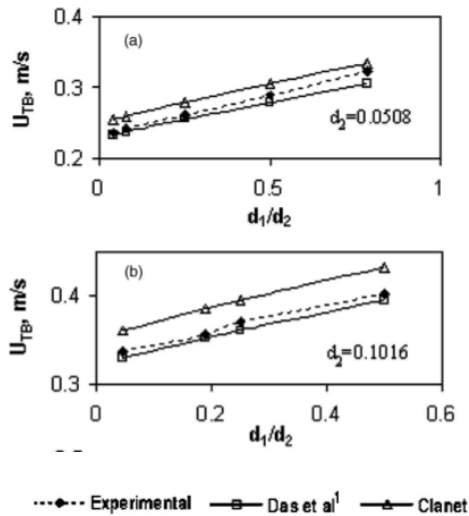


Figure 7. Agarwal et al (2007) Comparison of Model to Experimental Data

The values a and b come from geometric formulations proposed in Das *et al.* (2002). The value θ was calculated from a software called Image Proplus with striking accuracy:

d_2 (Outer dia in m)	d_1 (Inner dia in m)	Angle of wrap (θ in radian)	
		Calculated	Measured
0.0508	0.002	8.32	*
0.0508	0.004	6.94	*
0.0508	0.0127	5.85	6.0
0.0508	0.0254	4.73	4.75
0.0508	0.04	3.48	3.5
0.1016	0.0045	6.31	*
0.1016	0.01905	7.23	*
0.1016	0.0254	5.75	5.8

Figure 8. Comparison of Bubble Wrap Found in Experiments to Predictions by Image Proplus Software by Agarwal et al (2007) Using Water and Air

As can be seen in the current literature, the velocity of bubble rise in the concentric annular geometry is governed by similar properties as in the round geometry. Froude Number seems to be the prime governing factor in bubble rise velocity in both situations. Though it is more complex and harder to quantify, the geometry of the Taylor bubble – the curvature of its nose section – can approximately determine the bubble rise velocity. However as was seen when higher viscosity fluid was introduced to round pipes, non-Newtonian fluids of higher viscosity can affect the bubble's migration.

2.4. non-Newtonian Fluids

As with annular geometries, relatively less investigation has been invested into the behavior of Taylor bubbles in a stagnant surrounding of non-Newtonian fluid; even less into the effect of fluid yield point on gas migration in annular geometries. However, some focus has been devoted to this area more recently.

Rader *et al.* (1975), alongside their previously discussed work on the effects of viscosity and geometry on bubble rise velocity, they investigated the effects of apparent viscosity of non-Newtonian liquids. Of interest, they investigated the effect of yield point of Bingham-Plastic fluids. Through this investigation, they found bubble rise velocity could be modeled as such:

$$v_{LB} = \frac{52(\rho_L - \rho_g)(d_2 - d_1)^2}{\mu_p} - \frac{5\tau_y(d_2 - d_1)}{\mu_p} \quad (\text{Laminar}) \quad [25]$$

$$v_{LB} = \frac{132(\rho_L - \rho_g)^{0.56} (d_2 - d_1)^{0.69}}{\rho_L^{0.44} \mu_p^{0.12}} \quad (\text{Turbulent}) \quad [26]$$

where d_1 and d_2 are the diameters of the inside and outside annulus bounds, respectively. ρ_L and ρ_g are the densities of liquid and gas bubbles, respectively. τ_y is the yield point of the fluid, μ_p is the plastic viscosity of the fluid, and v_{LB} is the rise velocity of the bubble.

Johnson and White (1993) analyzed the effects of non-Newtonian viscosities, annular geometry, and various inclination angles on gas migration in fluid flows. The authors used 2 Xanthan gum solutions of different yield stresses, using the Herschel-Bulkley Rheological Model. They found that “when air is injected into more viscous, non-Newtonian, shear-thinning, fluids the gas migration is almost entirely by large (Taylor) bubbles... For fluids with an effective yield stress there will be small bubbles which will be held in suspension and will be transported with the liquid flow.” This seems to imply that small bubbles may be entrained in static fluid, leading to a rise velocity of zero at certain yield point and bubble size thresholds.

Carew, Thomas, and Johnson (1995) analyzed the rise velocity of bubbles in various diameter pipes at various inclinations. They included both Newtonian and non-Newtonian fluids but did not consider annular geometries. They found that “in near vertical pipes, the bubbles behave as if they were in Newtonian liquid possessing an apparent viscosity appropriate to the local strain-rate near the bubble nose.” They developed some very complex models that closely approximated rise velocity through Herschel-Bulkley fluids.

The idea was put forth by Dubash and Frigaard (2002) that a balance point between bubble size and the yield point of a Herschel-Buckley or Bingham Plastic fluid could be reached at which point, the relative velocity between fluid and gas is zero. Essentially, the buoyant forces on the gas bubble must overcome the yield point before the bubble will propagate. They followed up this work with experimental investigation in 2007. In their 2002 derivations, Dubash and Frigaard proposed that in a viscoplastic fluid, a bubble migrates when its Bingham Number is below a certain threshold:

$$B < \frac{[V_b U_b]^{1/2}}{2\text{meas}(\Omega)^{1/2}} \quad [27]$$

where $\text{meas}(\Omega)$ is the surface area of the bubble, V_b is the Volume of the bubble, and U_b is the bubble velocity in a Newtonian Fluid. In their context, Dubash and Frigaard defined viscoplastic fluids as “...a material that behaves locally as a rigid solid if a certain (yield) stress is not exceeded in the fluid.” Thus, when the Bingham Number is above said threshold, the bubble will not migrate. Relevant to the interest of this literature review, they extended this statement to cases of asymmetric bubbles; which can’t be directly applied to annular geometries but is relatively close. “For an axisymmetric bubble propagating steadily at speed U_b , with radius given by $r=f(z)$, $U_b=0$ if

$$B > B_{c,a}$$

$$B_{c,a} = \frac{1}{2\sqrt{2}}(z_+ - z_-) \left(1 - \frac{2\pi\beta}{V_b} \int_{z_-}^{z_+} \frac{f' [f'' f - (f')^2 - 1]}{[(f')^2 + 1]^{3/2}} dz \right) \quad [28]$$

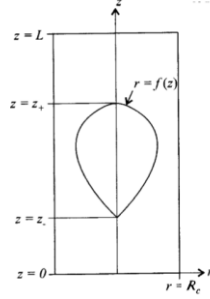


Figure 9. Axisymmetric Bubble in a Cylindrical Column.

where β is the dimensionless surface tension coefficient $\beta = \frac{\varepsilon}{\rho_l g R^2}$. f refers to function of $r=f(z)$. As stated above, this can't be directly applied to annular geometries, given the previously discussed geometric behavior of bubbles in annuli. However, Dubash and Frigaard went on to propose "*Theorem 6*. Suppose $\beta=0$ and we consider an infinite domain Ω . If $r=f(\theta, z)$ denotes a bubble surface which is static for fixed B , then for $\lambda < 1$, $r=\lambda f(\theta, \lambda z)$ denotes a smaller bubble of the same shape. The flow around this bubble is also static." Thus, if one could approximately model the complex "wrapping" shape that bubbles have been shown to assume in annular geometries, then perhaps a critical Bingham Number could be found, by following Dubash and Frigaard's proofs, above which the bubble will not migrate through the liquid because of its yield point.

In their experiments that followed, shared in 2007, they had a very hard time controlling fluid variables and precisely approaching the limits they hypothesized in their previous paper. They found that as they approached the Bingham Number limits of which they were interested, they could not get the bubbles to detach from the injection device; the bubble needed an additional buoyant force. This finding, while not precise, provided an approximate validation to their theorems.

A very rigorous mathematical solution to the bubble rise in non-Newtonian fluids was put forth by Dimakopoulos *et al* (2013) using and comparing Advanced Lagrangian Method and Papanastasiou Model. They state that bubble rise can be reported as a velocity or in terms of the corresponding Reynolds and Weber Numbers resulting for it. "For a shear thinning fluid these are defined as follows:

$$Re = \frac{2R_b^{*n} \rho^* U^{*(2-n)}}{k^*} = 2^n Ar U^{(2-n)}, \quad [29]$$

$$We = \frac{2R_b^* \rho^* R^{*2}}{\gamma^*} = 2ArBoU^2. \quad [30]$$

where Ar is the Archimedes Number, Bo is Bond Number, U is bubble velocity, k is the consistency index of a Herschel-Buckley fluid, and n determines whether the fluid is shear-thickening or shear-thinning. In addition to these, they refer to the drag coefficient, C_d , as a description of the resistance to bubble flow by the fluid.

$$C_d = \frac{2F^*}{\rho^* U^{*2} \pi R_b^{*2}} = \frac{2F}{\pi Ar U^2} = \frac{8}{3Ar U^2}, \quad [31]$$

where F is the dimensionless drag force on the bubble surface. For a steadily rising bubble, F equals the buoyancy force, $4\pi R_b^{*3} \rho^* g^* / 3$, which is easy to calculate given the volume. They used the above descriptors to compare predicted values with measured values in previous studies. More to the point of their work, however, they found that, in general, “the Advanced Lagrangian Method predicts accurately the yield surfaces either away from the bubble or ... around its equatorial plane...” They also found that the Papanastasiou model was effective near critical conditions and could be used suitably to find the critical Bingham Number. “Moreover, the detailed flow field and the yield surface are accurately determined with the Papanastasiou model for small and intermediate Bingham numbers...” They showed, definitively, that fluid elasticity of fluids like Carbopol lead to differences in shape previously attributed to viscoplasticity or shear-thinning by authors including Dubash and Frigaard.

Most of the discussed investigations were concerned with basically open upward flow, where both phases flowed concurrently upward; some would flow the liquid phase, others kept the liquid phase stagnant. All allowed mass flow out of the control volume. A distinct gap seems to exist in the literature for a situation which is directly related to well control situations; that being the situation in which an annulus full of a fluid that can be characterized by the Hershel-Bulkley or Bingham Plastic model (one with a yield point greater than zero) has a gas bubble migrating upward while the annulus is shut-in (i.e. a closed system). In application, that refers to a gas bubble migrating upward either in a shut-in well or in a very deep, vertical section of a well.

Chapter 3. Statement of Problem

Whilst conventionally drilling a well, the in-situ fluids trapped in pores between rock grains are controlled (i.e. kept from entering the wellbore) by use of drilling fluid. This fluid is often a mixture of particulate weighting additives meant to increase the liquid's density and viscosifying agents to help suspend those particulates. The increase in density allows for the fluid to control higher pressures at the deepest point in the well via the fluid's hydrostatic pressure. However, if the drilling fluid exerts less pressure on the reservoir fluids than the surrounding rock exerts on the reservoir fluids (i.e. if pressure inside the wellbore is less than the pressure outside the wellbore), the reservoir fluids will flow into the well. This is commonly known as a kick, a sudden, uncontrolled influx of reservoir fluids. This situation is also referred to as a loss of well control because the density of the fluid in the well is no longer known throughout the system and the fluid in the wellbore must be replaced with higher density fluid to control the higher than expected formation pressure.

Once a kick has been recognized, the well must be shut in at surface to regain control of the well. At this point, a decision must be made on how the driller wants to approach the problem of removing the influx. There are multiple influx removal methods that provide pros and cons with respect to wellbore pressures; equipment ratings, equipment capabilities, and formation strengths are all considerations that must be weighed in this decision. However, in the context of a gas kick, any time that is spent decision-making is time that the gas will be migrating towards the surface.

Grace *et al* (1996) consolidated 5 real-world examples of gas migration during kicks. They mention in the introduction to their paper, "historically, field personnel have used a "rule of thumb" that gas migrated at the rate of 1000 feet per hour." However, through their investigation they found migration rates of gas kicks in shut-in wells that varied between 1.5 ft/hr to 1339 ft/hr. They included one well with a 11.2 ppg gel polymer drilling fluid system that was characterized with a Plastic Viscosity of 29 cP and Yield Point of 29 lb/100 ft²; in this situation, an inclined well (39°) allowed a 12-barrel gas influx migrated upwards in the annular space at an upward velocity (along the wellbore) at 1339 ft/hr. In water systems, the highest rate of migration was 784 ft/hr.

These situations give rise to the question of what effect fluid properties, geometries, and pressures are having on the uncontrolled migration of the gas kick.

Chapter 4. Test Matrix

4.1. Experimental Setup

These experiments were performed in a newly built and custom designed flow loop, designed and built by Mohammed Bousaleh and Nick Henry. This flow loop consists of a vertical 4-inch Schedule 40 (4.5" OD, 4.026" ID) main pipe body, 21.3 feet in length, with a 2-inch Schedule 40 pipe (2.375" OD, 2.067" ID) in the center of the pipe, a gas flow system, fluid flow system, and data acquisition system. These systems work together to either allow continuous flow in the main body for analysis of transient or steady state flow regimes or closed end gas migration analyses, such as those considered in this paper.

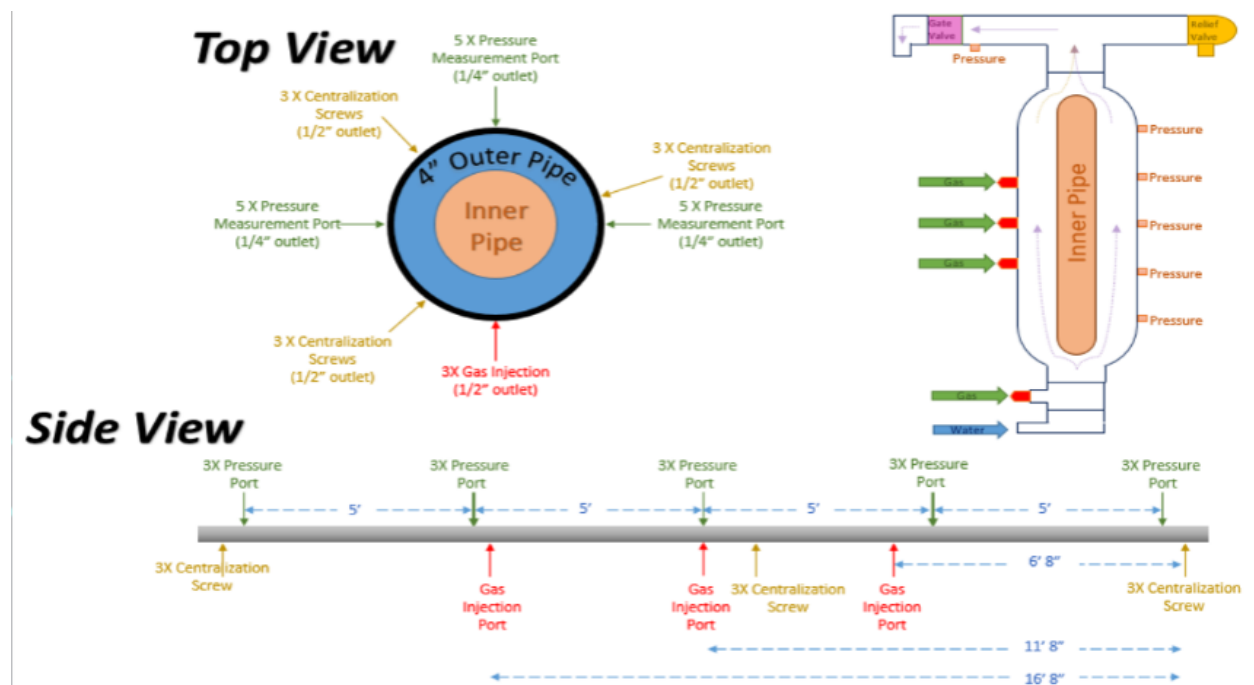


Figure 10. Main Flow Annulus Schematic (Mohammed Bousaleh)

The main flow conduit consists of a vertically oriented 4-inch Schedule 40 pipe (4.5" OD, 4.026" ID), 25-feet in length. The pipe has 3 levels of threaded ports available for gas injection (at 5' intervals) and 4 levels of ports for pressure transducers at intervals of 5-feet. At the base of the pipe, a ball valve serves to close in a defined volume of fluid and provide protection to the pump and fluid manifolds as pressure increases in the main flow annulus. At the top of the pipe, a tee directs the flow to a pressure relief valve on one side and a fully closeable gate valve on the other. The pressure relief valve is set to 90 psig to provide a high safety factor and protection for the upstream equipment. The gate valve serves its normal purpose - as a fully closeable gate valve, but also will act as a choke for outflow while gas flows into the system. Beyond the gate valve, liquid released from the system is directed to a 2" clear PVC cylinder with graduation marks that is used to measure the amount of fluid

displaced from the main flow annulus as gas is allowed into the system; an indirect measure of the volume of the bubble.

The gas flow system, from gas generation to flow conduit, consists of an air compressor and bubble chamber. Unfortunately, before experiments could begin, most of the high voltage equipment associated with the experimental setup (25 HP progressive cavity pump and high capacity air compressor) were disallowed from use while the lab facility was undergoing improvements. The air compressor used was a Husky 8 Gallon 'Hotdog' Air Compressor; it is rated for a maximum pressure of 150 psi. Connecting the air compressor to the bubble chamber is a customized connection that allows the experimenter to incrementally add air to reach a target starting pressure. For the purposes of these experiments, a custom bubble chamber has been built and inserted in-line between the gas manifold and main flow annulus. This bubble chamber is a combination of pipe and ball valves. An analog pressure gauge allows manual reading of pressure in the chamber; an electronic pressure transducer allows monitoring and recording of the chamber pressure. The bubble chamber has a measured volume of 211.145 in³, about 0.9 gallons.

Chamber pressure is the primary metric used to control bubble mass and bottom hole pressure at the beginning of the experiment. Based upon mass conservation, the mass removed from the bubble chamber must be equal to the mass allowed into the flow annulus. Furthermore, we must know the starting and ending pressures for the chamber; based on the knowledge that a target bubble size and target pressure at the top of the system are desired.

$$P_{bh, start} = P_{system, start} + \rho_{fluid} * g * y_{system}$$

$$-\Delta m_{chamber} = m_{bubble}$$

$$m_{chamber, i} = \frac{P_i V_{chamber}}{z_i T * R_{air}}, m_{bubble} = \frac{P_{liquid} V_{bubble}}{z_i T * R_{air}}$$

At the Pressures and Temperatures being considered, Air is considered an ideal gas, so the z factors will be disregarded.

$$\Delta m_{chamber} = \frac{V_{chamber}}{T * R_{air}} (P_i - P_f)$$

$$P_f = P_{bh, start}$$

$$P_{i, chamber} = P_{system, start} + \rho_{fluid} * g * y + \frac{T * R_{air}}{V_{chamber}} * m_{bubble}$$

The fluid flow system consists of fluid tanks, a positive displacement pump, fluid manifold, and flexible hoses. Two fluid tanks, 36" diameter, are individually isolated from each other and allow containment of 100 gallons, each. A suction hose, a flexible hose with reinforcement against radial collapse, connects the tanks to the fluid inlet of the pump. The pump is a Honda Trash Pump, powered by an 11.7 hp Honda GX 390 engine, capable of 580 gpm and 95 foot of total lift; it does not provide much by way of pressure support, but serves the purpose of circulating and placing test fluid into the flow annulus. The pump is connected to a fluid manifold made up of 2-inch, Schedule

80 galvanized steel, with a Rosemount 8700M Magnetic Flowmeter installed in-line to measure the fluid flow rate; this flowmeter is calibrated to be accurate from 0 to 30 ft/s. 2-inch flexible hoses, rated for 200 psi, connect the pump to the manifold, the manifold to main flow annulus, and from the 2 outlets (primary and emergency) of the main flow annulus back to the tanks. A burst-type pressure regulator, set to 90 psig, is installed at the top of the main flow annulus to protect the upstream equipment.



Figure 11. Front View of Experimental Setup

The Data Acquisition System consists of pressure transducers, fluid flow meter, a gas flow meter, and a Data Acquisition program that collects the data. Pressure transducers are placed throughout the system to monitor key variables; one on each of the manifolds and 5 along the main body of the main flow annulus. The pressure

transducers emit a voltage between 0-10 Vdc directly correlative to a pressure range of 0-150 psig. The fluid flow rate is measured via the Rosemount 8700M Magnetic Flowmeter. The gas flow rate is measured via the Rosemount 3051SF Orifice Flowmeter. All measurement instruments are fed into a junction box near the main flow annulus from which a single Ethernet cable transfers all data signals to a laptop computer on which the Data Acquisition Program presents and writes the data to files. The Data Acquisition program (DAQ) is built using a National Instruments LabView software package.

The above summarizes the equipment that will be used to create the test environment. The goal is to enclose a known volume of water (2246.969 in³) in an annular geometry under a known pressure and to release a Taylor Bubble into the system and to measure the vertical migration rate of the bubble as it rises through the non-Newtonian fluid. Multiple system pressures will be tested, as well as multiple fluid characteristics. However, because the primary flow annulus is not made of a transparent material, a method of data interpretation will need to be implemented to derive the relevant information; this will be explained in Section 4.3.

Experimental Design Matrix		
Effect of non-Newtonian Rheology on Annular Gas Migration Rate		
Hypothesis As yield point increases, gas migration velocity will decrease, given an identical annular geometry.		
Materials Xanthan Gum Water		
Independent Variables – only 1 changed per experiment Xanthan Concentration (changes yield point and plastic viscosity of fluid) Initial system pressure		
Levels of Independent Variables	Xanthan Gum Concentration (affects Rheologic Model Adherence) 0.0%, 0.25%, 0.5%, 0.75%, and 1.0% (by mass)	Initial System Pressure at Top of Annulus <ul style="list-style-type: none"> • 10 psig • 30 psig • 60 psig
Number of Repeated Trials	5	3
Dependent Variable Gas migration velocity		
Controlled Factors Gas used = air Bubble Mass (target) = 0.004 lbm Closed System		
Control Results will be compared with a base set of experiments with water and air		

4.2. Experimental Procedure

The experiment consists of 3 main tests, performed simultaneously. The first 2 tests were not originally planned when these experiments were proposed. However, after a round of over 100 tests, it was found that due to the high yield stress exhibited by the fluids with higher concentrations of Xanthan Gum, the fluids retained a base level of air bubbles that were effectively irreducible. Due to this, the fluid was very compressible, compared with water. Pursuant to this finding, we planned to implement a procedure of testing the fluid's compressibility before each run.

The first test is a 'compression test' that aims to find the compressibility of the fluid through pressurization and the resulting change in fluid density. In this test, the flow annulus is isolated and is pressurized from atmospheric pressure to about 50 psig; the change in density and change in pressure are recorded and used to estimate an average fluid compressibility of the fluid in the flow annulus.

The second is a 'decompression test' that aims to find the compressibility of the fluid through volumetric expansion. In this test, the flow annulus is isolated (the annulus volume is known) and the gate valve at the top of the flow annulus is slowly opened, allowing the fluid (having been pressurized from the previous test) is allowed to expand and reach atmospheric pressure at its highest point; the excess fluid is captured in the graduated cylinder downstream of the gate valve at the top of the flow annulus. The difference in fluid levels of the graduated cylinder is recorded; the change in pressure and volume will be used to estimate an average fluid compressibility of the fluid in the flow annulus.

The third test is the primary test of interest; in this test, a bubble of target mass is released into the annulus and closed in at a target system pressure. Before the test, a hose connected to the outlet of the annulus is filled with test fluid until some fluid is showing in the graduated cylinder at the top of the setup; that level is recorded. The annulus is then completely shut in. The bubble chamber isolation valve is opened to allow communication between the bubble chamber and the annulus. The gate valve at the top of the annulus is then slightly opened to allow system liquid to flow out of the annulus into the hose and graduated cylinder; the action of system liquid flowing out allows gas to flow in. When the bubble chamber target pressure is reached, the gate valve is closed, then the bubble chamber and flow annulus are isolated by the isolation valve. At this time, the bubble will already have begun its rise through the annulus; this rising action is captured by the increasing trend in system pressure via pressure transducers and recorded to a data file. As the bubble is rising, the experimenter takes the final reading of the graduated cylinder to find the total volume of fluid that flowed out of the system (i.e. the volume of bubble allowed into the system). Time and temperature readings are also taken every run to enable proper estimation of the mass of gas allowed into the system. Used fluid is not allowed to mix with unused fluid.

To improve data collection and validity of measurements, samples are drawn from the fluid at 4 times throughout the experimental procedure; samples are taken before the fluid ever enters the system and has the large bubble introduced, after the 3 tests at 10 psi system pressure, after the 3 tests at 30 psi system pressure, and after the 3 tests at 60 psi system pressure. Each of these samples are measured for density

and rheology (on an electronic mass balance & Fann Viscometer, respectively) on site, within 5 minutes of the sample's capture from the tank. Each of these samples are marked for their apparent volume in the sample cup and kept in a climate-controlled office after capture; these samples are checked a few days later to see if their volume has changed – often the bubbles are released very slowly.

4.3. Data Interpretation

Many previous authors use transparent flow loops to measure the migration rate of bubbles in fluids. However, the exiting flow loop is made entirely of non-see-through materials. Thus, it is impossible to make visual measurements of the dynamics of the system. However, given the data that can be acquired, a method of analysis can be developed to develop the desired information.

The initial mass of gas allowed into the system will be an important parameter to control. Given the volume of the bubble chamber, we can measure the difference between initial and final bubble chamber pressures to calculate the mass of gas allowed into the system as well as by the volume of fluid displaced during bubble ingress, by way of the graduated cylinder at the system outlet.

To measure the rate at which the gas rises in this closed system without any visual confirmation, the main parameter that will be measured and analyzed will be the pressure. The rate of change of the pressure is the direct result of gas migration. Based on the common model used for well control, the following simplifying assumptions are normally made:

- Friction is neglected
- the fluid is incompressible
- the bubble occupies the entire flow area and remains contiguous all the way up the well
- given that pressures will not rise above 100 psig, gas density is small enough to be negligible

Given the assumptions, the volume of gas allowed into the system will be the same at the point of gas inlet into the main flow annulus as it will be at the top. When the bubble is initially allowed into the main flow annulus

$$P_{top} = P_{bubble} - \rho g z$$

where P_{top} is the pressure at the top of the main flow annulus, P_{bubble} is the bubble pressure, ρ is the fluid density, g is the gravitational constant, and z is the vertical measure of distance between the topmost pressure transducer (where P_{top} is measured) and the top of the bubble; the sign convention is downward, in the direction of gravity. When the time derivative is taken of this simple equation, it shows that the change in pressure at the top of the main flow annulus at infinitely small time increments is directly related to the velocity of migration of the constant pressure bubble.

$$\frac{dP_{top}}{dt} = -\rho_f g \frac{dz}{dt}$$

$$-\frac{dz}{dt} = \frac{-1}{\rho_f g} \frac{dP_{top}}{dt}$$

It is important to note that the negative sign on the right-hand side of the equation is due to the sign convention used to establish the Pressure-Position relationship in the hydrostatic equation. Thus, we have a direct measurement of the bubble velocity so long as the assumption of liquid incompressibility holds.

However, due to the procedures used in executing the experiments and the high yield stresses exhibited by the fluids, the assumption of fluid incompressibility was not valid. This led to a complete overhaul of experimental and analytical processes. As discussed in Section 4.2, compressibility is measured by filling the system with test fluid, pressurizing it to 60 psig, then releasing the pressure through the outlet valve and measuring the expansion of the fluid.

$$C_f = -\frac{1}{V} \frac{dV}{dP}$$

Hence, the pressure growth due to bubble rise velocity cannot be directly applied to find the bubble velocity. Instead, the difference in the pressure readings from pressure transducers along the pipe can give a strong indication of the bubble's location. When the bubble enters a section between 2 pressure transducers, separated by a known vertical distance, it significantly decreases the effective density of the fluid acting between the pressure transducers. This can be seen in the data as a significant decrease in the pressure difference between any 2 pressure transducers between which the bubble is located. By comparing the time when the bubble enters and exits all sections (areas between the pressure transducers), we get a direct measurement of the bubble rise velocity; neglecting acceleration effects. As should be expected, the compressibility of the fluid depresses the calculated bubble rise velocity compared to the incompressible model, given the same bubble rise velocity.

4.4. Sources of Error

Every experiment is designed to isolate and measure as few parameters as possible. Pursuant to this goal, error needs to be considered and accounted for. In this set of experiments, the following sources may have influence over experiment results:

1. Gas retention in fluid: The largest source of error is the fluid, itself. Because of the batch sizes needed, mixing technique, and lack of a vacuum pump, the fluids' yield stress caused some minimum level of gas entrainment; this gas entrainment effect is the cause of the compressibility issues and is the primary reason for the changes that were made to the experimental design. These effects can be accounted for.
2. Fluid Outflow Control: Because of the height of the experimental setup, the gate valve that will allow fluid outflow sits about 30 feet above ground level. It is controlled by a long steel rod with a "steering wheel" at the end. This allows the experimenter to watch the analog pressure gauge on the bubble chamber and close off the fluid outflow when the chamber pressure reaches target pressure; calculated before each run to allow in a consistent mass of gas. The source of

error is in the precision of the analog pressure gauge (range 300 psig) and the rate at which pressure falls when allowing the bubble in to the flow annulus. For the high-pressure tests, the system pressure falls very quickly, making it very hard to control the pressure at which the outflow is stopped.

3. Graduated Cylinder: The graduated cylinder that is used to measure the amount of fluid that is displaced by gas during the outflow process is a custom-made, clear PVC pipe with graduation marks every 1/8 inch. On a sunny day, the fluid level can be read within 1/32"; however, on cloudy days, 1/8" can be the max precision attained in volume measurements. That equates to an error of about 0.42 in³.
4. Pressure Transducers: The pressure transducers exhibit variance across the measured pressure. This can be filtered out by the Data Acquisition System via filtering, but that causes issues reading the data at the rates necessary to capture some of the transient portions of each experiment. This effect is instead handled in post-processing.

4.5. Fluid Selection

Fluid selection will have a significant influence on this investigation. Water will serve as the zero-yield stress control fluid. There are, however, many options available to achieve a fluid with a high yield point; of the types of fluids by which this can be achieved, focus will be placed on Carbopol, Xanthan Gum, PAC-R (a Polyanionic Cellulose-based polymer additive), and mixtures of Bentonite and Barite. Fluid consistency, price and availability, and environmental impact are the primary selection factors that will be considered.

Fluid homogeneity spatially and temporally will be very important for the results of this investigation. If fluid characteristics, particularly viscosity, vary along the length of the pipe, then the ability to accurately measure the variables of interest will be compromised. Particulate fluid additives, such as mixtures of Bentonite and Barite, tend to fall out of solution over time; this leads to a heterogeneity over the length of the pipe that must be avoided. Further, particulate accumulation on the lowermost ball valve could compromise the integrity of the seal over time. Because of this, polymer-based fluids, such as Carbopol, Xanthan Gum, and PAC-R will be preferred over particulate additives. The aforementioned polymer fluids exhibit shear thinning characteristics but are stable over time so long as the pH is at the correct level. Long chain polymers, like Xanthan Gum additives, will break apart in a centrifugal pump with negative effects to the fluid's rheological properties. This should not be an issue with a positive displacement pump, such that will be used here in these experiments; but it should be kept in mind as fluids are selected.

Additive price and availability will be another consideration in selecting the proper fluid. Bentonite and Barite are very commonly used while drilling wells, but as discussed above, the particulate fallout of the fluid essentially precludes their use in these experiments. Xanthan Gum is the most readily available of the polymer additives; it can even be bought at many Supermarkets in small quantities for its ability to be used in cooking. It is also readily available in bulk, online for around \$20 - \$40/lb, depending on the size of the order. Carbopol can be found online anywhere from \$20-\$70/kg

(~\$44-\$154 per lb). However, only a small amount needs to be used in any mixture. PAC-R is much harder to find; the only readily available online source online offered \$1500-\$3000 per metric ton, with a minimum order size of a kilogram. Due to availability, PAC-R may not be an attainable option. Xanthan and Carbopol can both achieve multiple Yield Points with different concentrations, so they should suffice for the needs of this investigation.

Of interest, Carbopol has a “fluid memory” which gives it a time-dependent quality that could raise issues; though Carbopol can exhibit a high yield point, after it has been sheared, that yield point will drop in subsequent tests. Xanthan gum solutions seem to exhibit more of an elastic tolerance to shear. Considering that fluid will need to be pumped into the main flow annulus for the experiments, shear in the pump body could have negative effects on the rheology of Carbopol solutions.

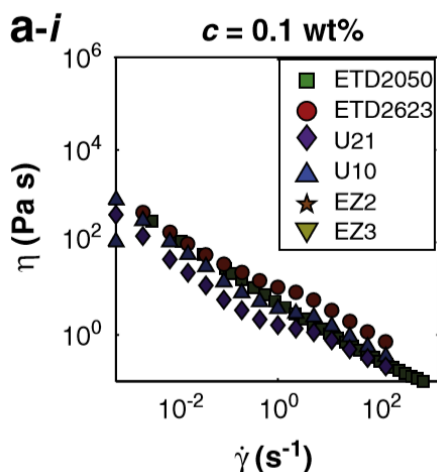


Figure 12. Relationship of Apparent Viscosity to Shear Rate Shows a Strong Drop Off as Shear Rate Increases. Carbopol does not recover its original rheology immediately. From Di Giuseppe et al (2014).

As seen in this section, solutions of varying concentrations of Xanthan Gum will serve to simulate drilling fluids of differing yield points. Xanthan is the most readily available and most versatile fluid we can select. Considering its use in cooking and food products, Xanthan will also be a good option in considering environmental impact.

Chapter 5. Results and Analysis

After 81 experiments were run over the summer of 2018, data analysis revealed that compressibility and stringing out effects were showing major effects on the results. Major differences between the bubble velocity found by pressure growth and the bubble velocity found by pressure transducer-to-pressure transducer inspection, final pressures showing departure from those predicted by the incompressible model, and concern over fluid controls led to need for a second round of experiments. The data set that resulted consists of 81 experiments of water and Xanthan mixtures of 0.25%, 0.5%, 0.75%, and 1.0% by weight. This section will review the results of said experiments starting at the individual experiment level, introduce the methodology used to analyze the influence of compressibility, and conclude with a look at the trends in the total data set.

5.1. Individual Experiment

A typical experiment can be exhibited on a graph of Pressure vs. Time. Important inflection points denote important events in the life of the experiment. Figure 13 shows a schematic of a typical experiment.

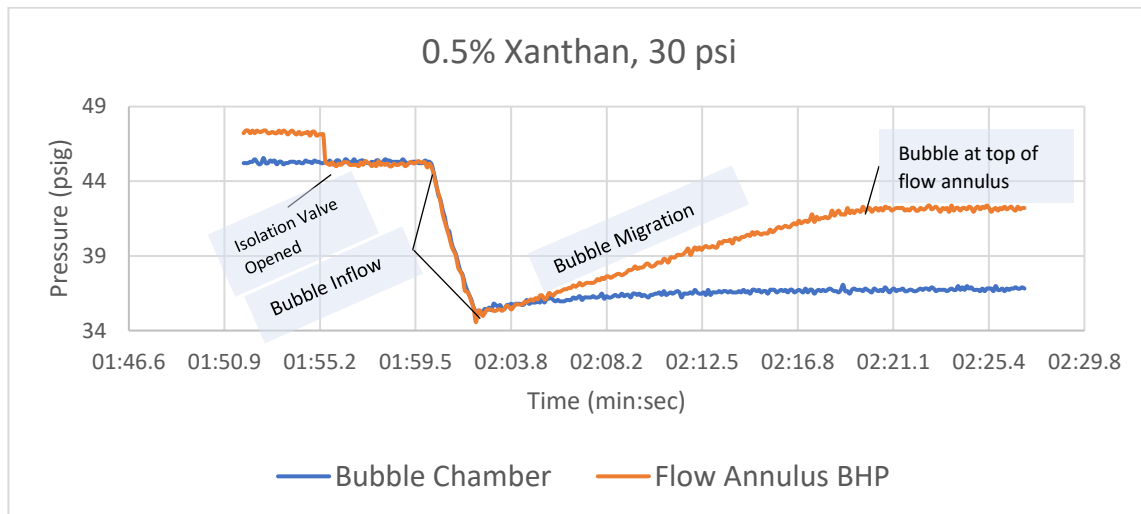


Figure.13. Pressure vs. Time Graph for a Typical Experiment.

As seen in Figure 13, the system shows an initial section of zero increase or decrease in pressure before a significant disturbance and equalization of pressures between the bubble chamber and flow annulus. The point of equalization is the point at which the isolation valve between bubble chamber and fluid-filled annulus is opened. The pressures decrease sharply as the bubble is allowed into the flow chamber; at this point, pressure differential at the top of the annulus is forcing flow out the gate valve that has been opened to allow outflow from the system – the flow out of liquid allows gas to flow in from the chamber to the annulus. The outflow gate valve is shut to close in the system and the isolation valve is quickly shut to minimize backflow of fluid into the gas chamber and to create a fully closed system for the bubble to begin its vertical migration. There may be a short section of acceleration, but the bubble and pressure trend reach terminal velocity very quickly; the increasing pressure trend becomes linear

and allows precise estimation of the pressure trend via linear regression – the minimum attained R^2 value was 0.970 on linear regressions of this linear section of pressure increase. The pressure transducer eventually flattens out to a consistent pressure once the bubble reaches the top of the system; this is often referred to as final system pressure. However, as discussed in previous sections, this experimental pressure trend includes the compressibility and string out effects.

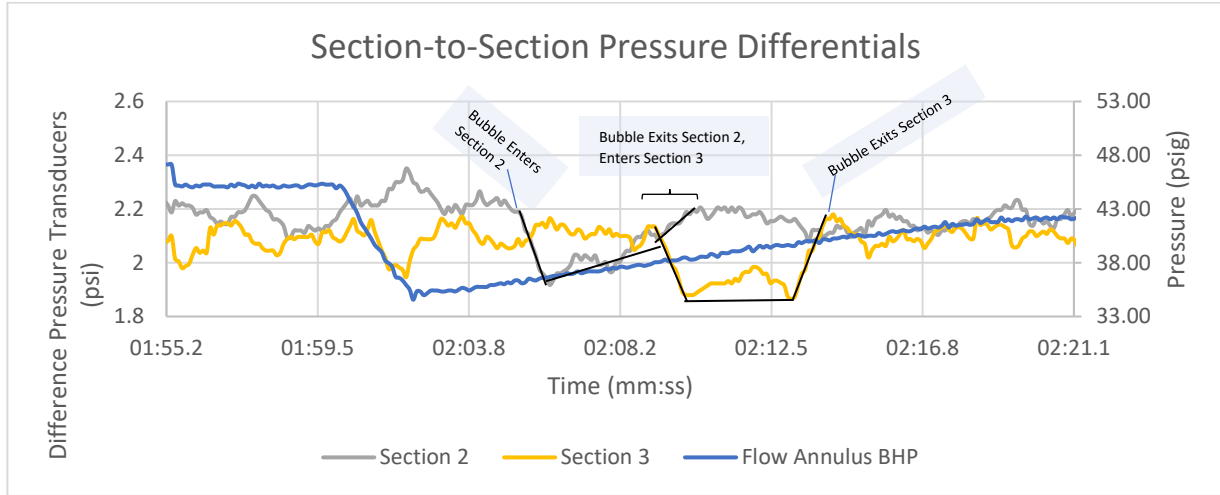


Figure 14. Section-to-Section Pressure Differentials Used to Find the True Velocity of the Bubble.

In order to get a direct measurement of the bubble velocity, the differences in each of the pressure transducers must be considered. The difference in pressure between the pressure transducers exists because of the hydrostatic pressure of the fluid in that section. When the bubble enters that section, the difference in pressure between those 2 pressure transducers will decrease because of the increase in void fraction – the volume within a given control volume that is not occupied by liquid. When the bubble moves from one section to another, the pressure difference should increase in the section from which the bubble is leaving and decrease in the section to which the bubble is migrating. Figure 14 illustrates a good qualitative example of this trend; to eliminate excess noise, only 2 sections are included. The important inflection points can clearly be seen as time increases; the bubble enters section 2, exchanges from sections 2 to 3, then exits section 3.

$$\Delta P_{sect,i} = P_i - P_{i+1} = \rho_{avg} g(z_{i+1} - z_i)$$

$$\frac{d\Delta P_{sect,i}}{dt} = (\Delta P_{sect,i})_t - (\Delta P_{sect,i})_{t-1}$$

$$\gamma = \left(\frac{d\Delta P_{sect,i}}{dt} \right) \left(\frac{d\Delta P_{sect,i+1}}{dt} \right)$$

$P = \text{Pressure}$

ρ_{avg} = average density of the section

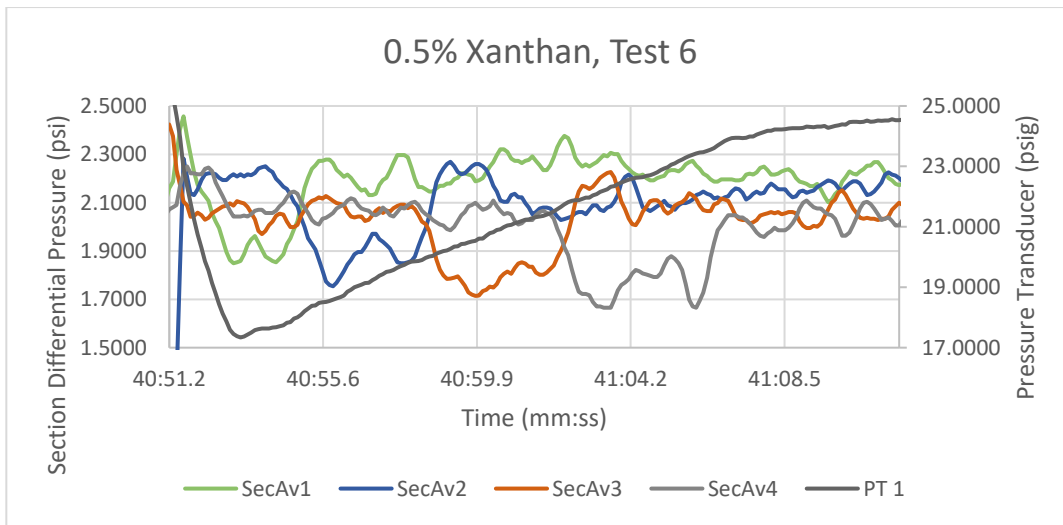
z = elevation of pressure transducer

i = Spatial Denotation

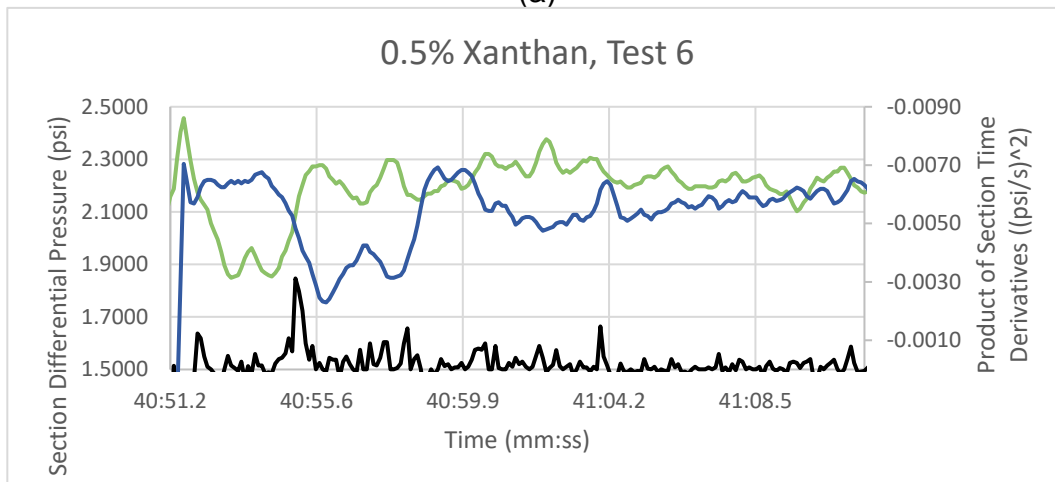
t = Time Denotation

$$\gamma = \text{Product of Time Derivatives of neighboring sections}$$

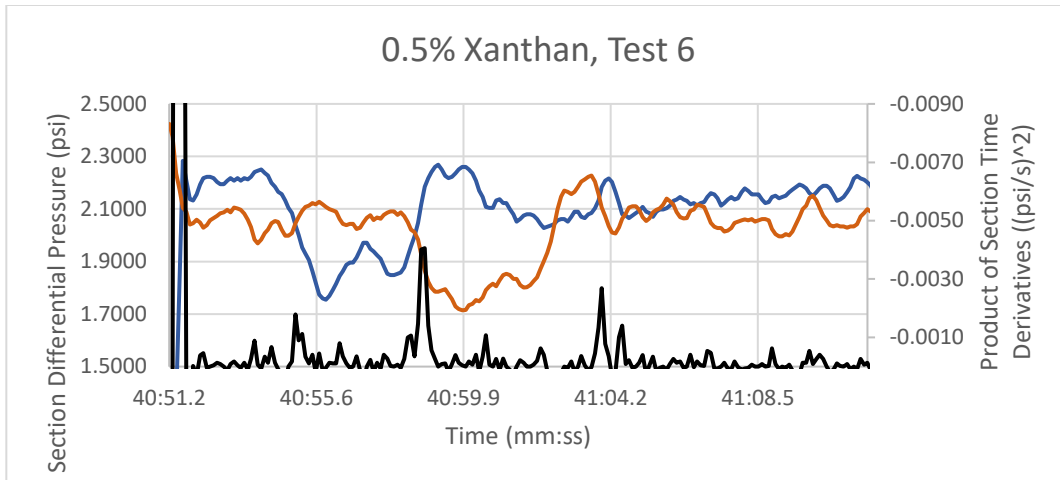
An alternate way to think about this section-to-section trend is through a time-series analysis of the differential pressures of each of these sections over the time that the bubble is known to be migrating. One can take the differential in time of the difference in pressure across a single section. That differential can then be multiplied to its neighboring section to find the time at which the bubble begins exchanging between 2 neighboring sections; because one section will be gaining bubble, it will be decreasing in density, the section losing bubble mass will be increasing in density at the same time. What one would expect is the product of the two time differentials to be negative. Because there is so much variability in each pressure transducer, and a difference is being taken between transducers to find the 'section differential pressure' that variability can be almost doubled. Filtering the data by trailing averages was implemented to better smooth the data. An example of the time series analysis can be seen in Figure 15.



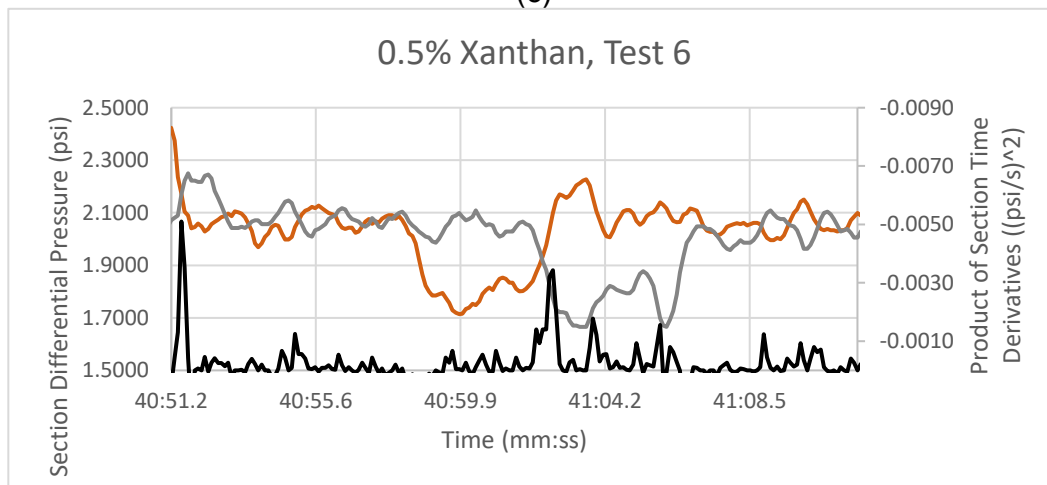
(a)



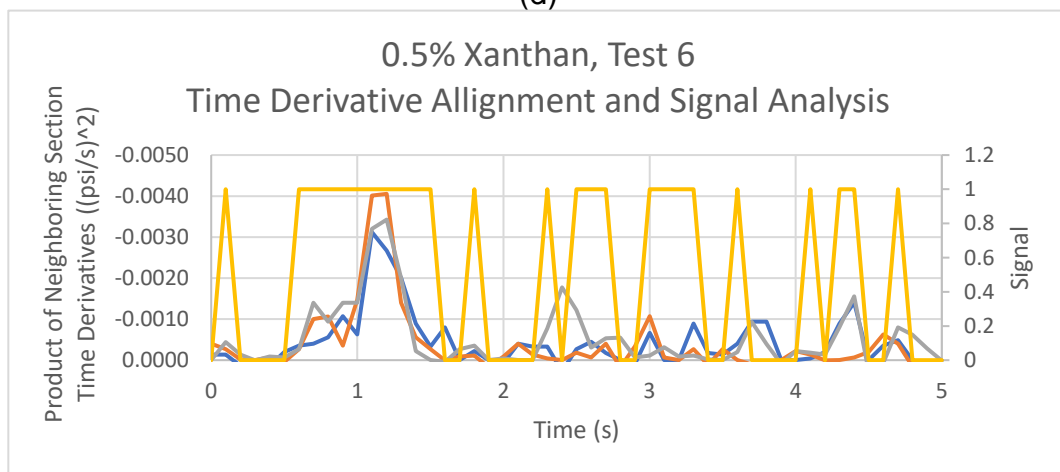
(b)



(c)



(d)



(e)

Figure 15. Exhibition of How Bubble Rise Velocity was Found through Time Series Analysis

(a) Total data set showing a single pressure transducer for context and all 4 sections together.

(b) Transaction of bubble between sections 1 & 2,

- (c) transaction of bubble between sections 2 & 3,
- (d) transaction of bubble between sections 3 & 4,
- (e) products of section time derivatives aligned (the peaks and apparent length of exchange are aligned to estimate time offset of bubble exchange between section interfaces) to compare the exchanges of bubble [signal refers to a Boolean operation measuring 1 when all 3 section-to-section interface products are negative]

By aligning the products of the time derivatives of each section-to-section interface, gives a good estimate of how long the bubble is in each section and how fast it is moving. Given distance between each interface is known, the velocity of the bubble can be found by dividing the distance between interfaces by the time it takes for the bubble to begin or end exchanging through interfaces.

Table 1 – Table of Inflection Points & Calculated Velocities

	Sect 1	Sect 2	Sect 3	Sect 4		
Bubble First Enters Section		40:54.4	40:58.1	41:02.0		
Entirely in Section		40:55.3	40:59.0	41:02.9		
Begins to Exit Section	40:54.4	40:58.1	41:02.0			
Entirely out of section	40:55.3	40:59.0	41:02.9		Average Velocity	
Bubble Nose Velocity (Entering Section)		1.351	1.282		1.317	ft/s
Bubble Tail Velocity (Entering Section)		1.351	1.282		1.317	ft/s
Bubble Nose Velocity (Leaving Section)	1.351	1.282			1.317	ft/s
Bubble Tail Velocity (Leaving Section)	1.351	1.282			1.317	ft/s

Once found, the true velocity of the bubble is used to estimate what the pressure growth rate of the closed-in system should be when the compressibility of the test fluid, measured before the experiment begins, is considered. In the case of the example shown, Test #6 performed on 0.5% Xanthan concentration fluid, when fluid compressibility is considered, the pressure trend and final system pressure closely adhere to the model; this was not consistently the case.

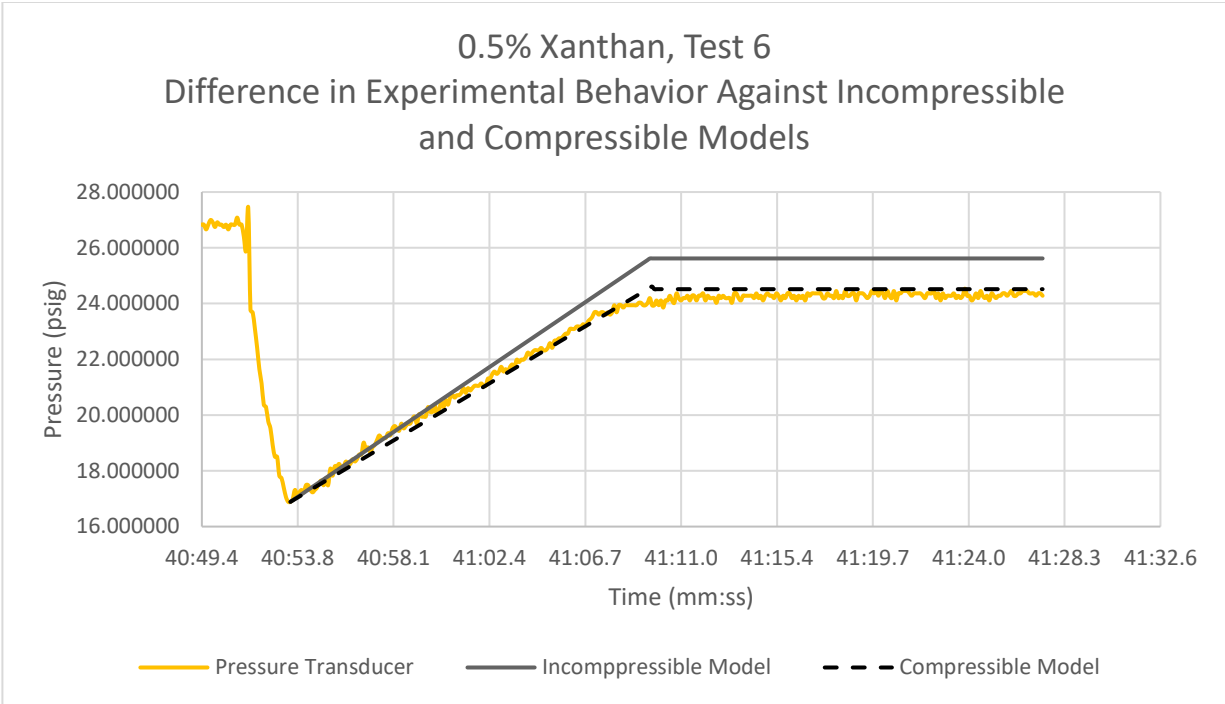


Figure 16. Exhibiting the Difference between a Typical Experiment and the Incompressible and Compressible Models.

Though in the above example case, chosen for its clear indications of bubble exchange, the final system pressure adheres very closely to that predicted by the compressible model, the experiments often deviated from the behavior predicted by accounting only for liquid compressibility, see Figure 17. In situations where deviation from the expected, compressible model of pressure growth is exhibited, the experiment must be violating an assumption. Because of the poor ability to control gas concentration in the base fluid, as explained in the Sources of Error Section, and because of the ability of the test fluid to trap gas bubbles, there is a possibility for the gas kick and test fluid to exchange mass. So, when the final surface pressure is less than that predicted by the compressible model, the gas bubble must be losing mass to the surrounding liquid; this is what one would expect in a situation where gas is stringing out along the well (string out effect). When the final surface pressure is greater than that predicted by the compressible model, the gas bubble must be gaining gas mass from the surrounding liquid. Using PVT calculations, comparing the expected final surface pressure against that which was attained, gives an estimate of the change in mass of the gas kick (gain or loss).

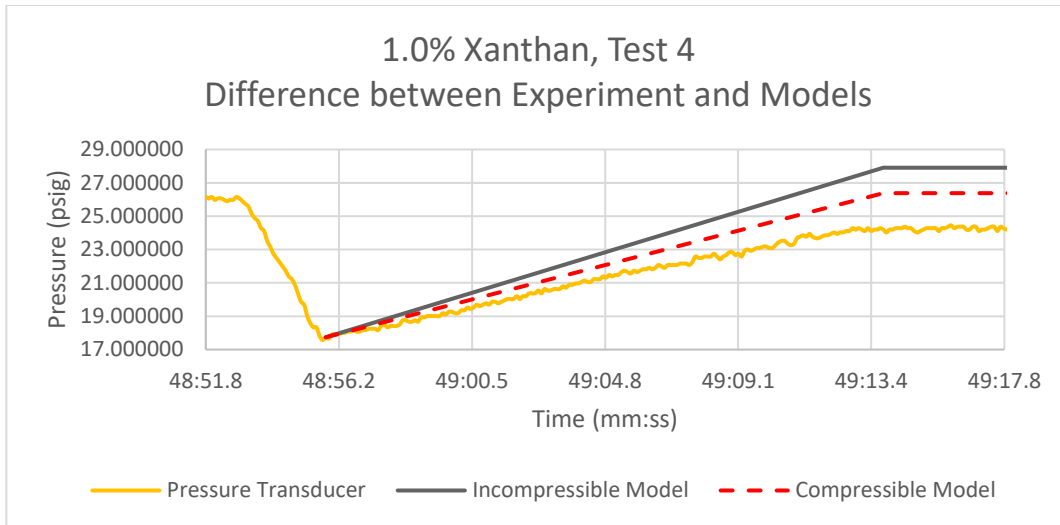


Figure 17. An Example of Gas Kick String Out. Bubble must be losing gas mass to the surrounding fluid

Comparing the results require an estimate of how the pressure growth should manifest, accounting for the known effect of compressibility; without an estimate of compressibility, it is impossible to isolate the possible stringing out effects.

5.2. Key Variables

Before looking into the data, some of the measurements taken need to be highlighted as the key variables in the analysis to follow.

Pressure transducer data is the primary measure that was taken during the experiments. Key points of inflection in the Pressure vs. Time series are gathered to serve as measurements for later analysis. When the bubble has been injected, the system shut in, the pressure at pressure transducer 1 (the transducer at the base of the system), is recorded and assumed to be a direct measurement of the gas bubble at bottom hole conditions; this pressure will be used in conjunction with the volume measurement to estimate the mass of gas injected into the system. Pressure Transducer 6 (The top-most pressure transducer) is assumed to be a direct measurement of gas bubble pressure when the bubble has reached the top of the system; this pressure will be used later to estimate the mass of bubble in its final condition. The top pressure transducer is used as the reference pressure for all liquid compressibility projections; in the decompression test, and volume outflow portion of the gas kick experiments, Pressure Transducer 6 is used to establish a liquid compressibility factor and compensate for liquid phase expansion during bubble injection, respectively.

The difference between each pressure transducer is used as a proxy measurement of fluid density during bubble migration. When only the liquid phase occupies the control volume between 2 pressure transducers, the difference between the two should be equal to the hydrostatic pressure across the vertical difference between the two pressure transducers. When the gas bubble is within that section, the

density will be much lower; the difference between the two pressure transducers will be less. This relationship will be used to determine where the bubble's location in the system and when the bubble enters or exits a given section.

A visual volume measurement is taken via the clear PVC graduated cylinder at the top of the experimental setup. The outflow leg is oriented such that all liquid outflow is diverted to the graduated cylinder. During every experiment, a liquid level is established in the outflow leg and recorded as the beginning fluid level, the final level is then recorded after outflow fluid is added during either fluid expansion during the decompression test or the bubble injection portion of the gas kick test. For the decompression test, the volume of outflow fluid is compared to the difference in starting and end point pressures of Pressure Transducer 6 to establish the relationship between fluid expansion and pressure. During the bubble injection portion of the gas kick test, the volume difference in the graduated cylinder, less the estimated fluid expansion/compression due to pressure difference recorded on Pressure Transducer 6, is the measured volume of bubble injected into the flow system.

5.3. Compressibility Simulation

Because string out and compressibility have such significant effects on the rate of pressure increase, in order to find the relative significance of their impact, each experiment was run through a custom simulation program that considered bubble velocity, bubble volume, fluid compressibility, and pressure in to account to project what the rate of pressure increase should have been if only compressibility was accounted for. With this, the aim is to isolate the effect of bubble string out.

The program runs as a fully explicit, iterative solver that holds the bubble velocity as a constant, while allowing the pressures and volumes balance each other for each of the timesteps, assuming a closed in system and modeling the test fluid as a contiguous, compressible fluid. Once completed, linear regression is performed on the simulation's pressure vs. time trend. This new pressure growth rate will be later compared to both the incompressible fluid model and experimental result to find the string out effect (see Figure 18).

Compressibility Simulation Program Flow Chart

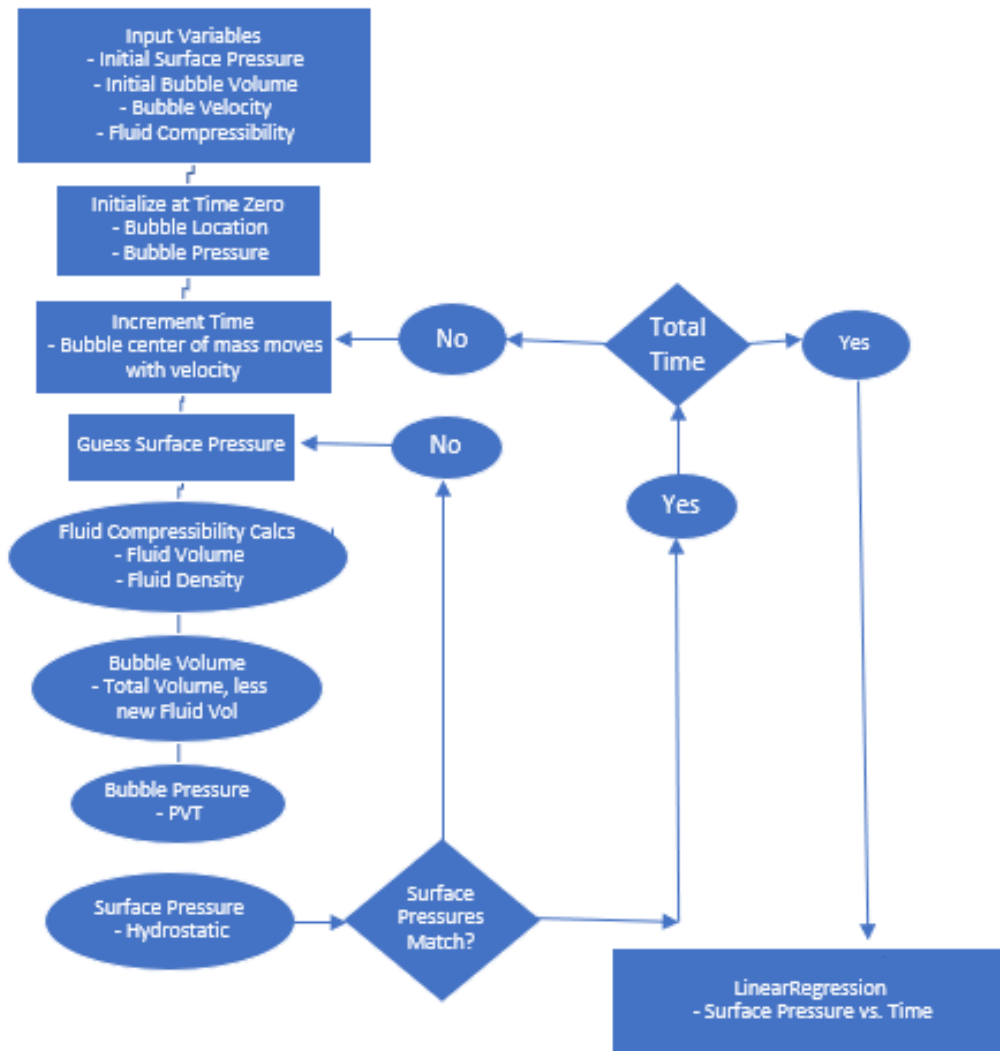


Figure 18. Compressibility Model Program Flowchart, Bubble Rise Velocity to Pressure Growth

The same process is done for the end state pressure; the compressibility model will have a lower end-state pressure than will the incompressible model; string out effect should depress that end-state pressure even further. Assuming no mass transfer between the test fluid and bubble, the end state pressure is a matter of whatever the initial conditions of the bubble (Pressure, Volume, and Temperature) and the compressibility of the fluid. The clear assumption made in this calculation is that any volume change in the bubble is a function of the compressibility of the surrounding fluid.

A similar program was devised, following the same approach in reverse, to find the true rise velocity of a bubble given the input of estimated liquid compressibility and linear pressure growth in the well. As for a field application, this program could have

direct application to any situation in which a gas kick has been closed in and a pressure reading can be taken over time. As can be seen in Figure 19, the program iterates upon a guessed true gas kick rise velocity until the resultant pressure growth agrees with the measured pressure growth.

Reverse Compressibility Simulation Program Flow Chart

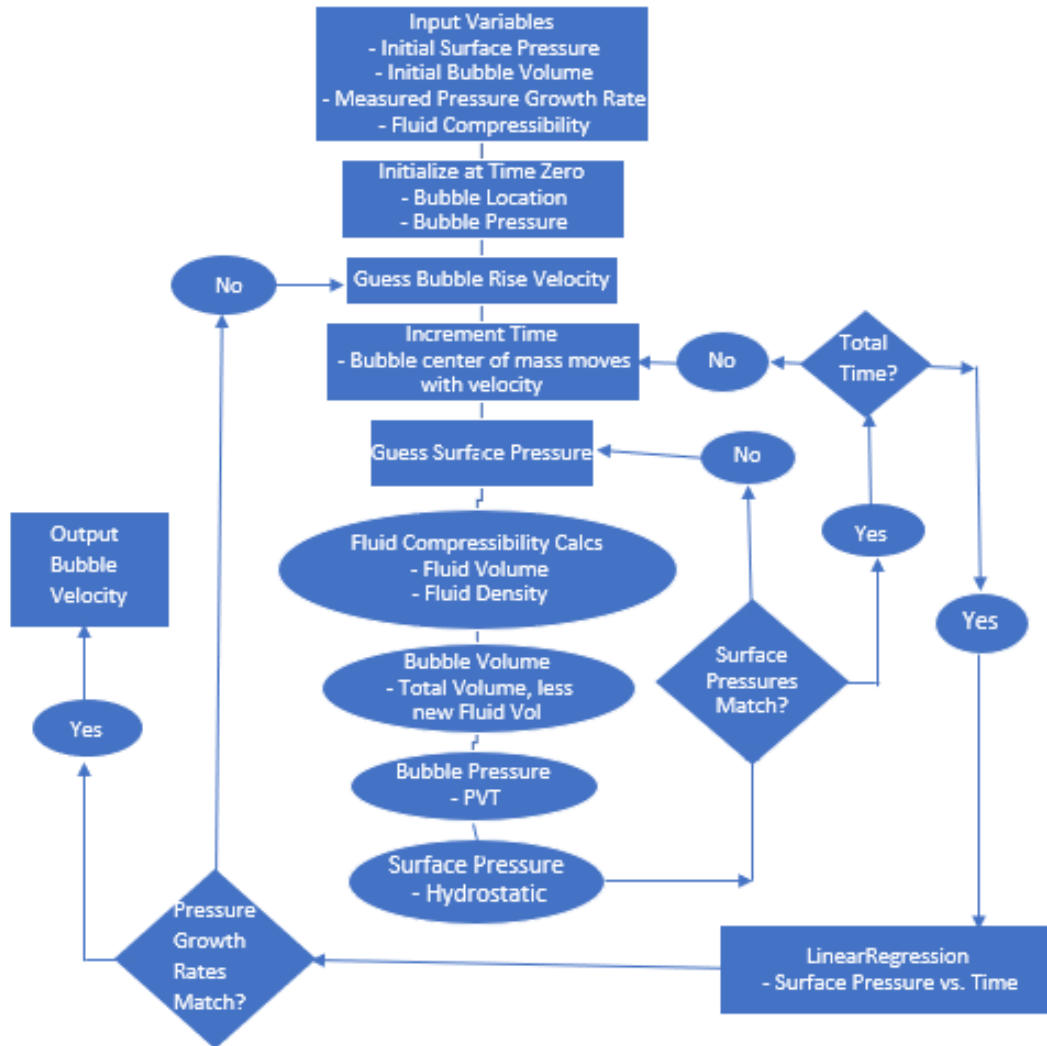


Figure 19. Compressibility Model Program Flowchart, Pressure Growth to Bubble Rise Velocity

After the experiments were run and these programs developed, further literature review yielded a set of equations that would simplify this approach and allow a simple excel program to run these estimates quickly. The equations, algebraic manipulations of the same set of equations and assumptions as those in the programs described above, came from a 1994 paper written by Petrobras engineers A.C.V. Martins Lage, E.Y. Nakagawa, and A.G.D.P. Cordovil. The equations are described below:

$$\frac{dP_s}{dt} = \frac{X_{go}V_{go}\rho_m g v_{slip} - q_g}{X_{go}V_{go} + X_wV_w + X_mV_m} \quad [32]$$

$$\begin{aligned} X_{go} &= \text{Initial Gas Kick Compressibility} \\ V_{go} &= \text{Initial Volume of gas kick} \\ \rho_m &= \text{Density of liquid} \\ v_{slip} &= \text{Gas kick rise velocity} \\ q_g &= \text{filtrate loss rate} \\ X_w &= \text{Formation (Well Walls) Compressibility} \\ V_w &= \text{Well Wall Volume} \\ X_m &= \text{Mud (Liquid) Compressibility} \\ V_m &= \text{Mud (Liquid) Volume} \end{aligned}$$

$$P_s = \frac{1}{X_m} \ln \frac{V_w - V_{go}}{V_w - \frac{P_{go}V_{go}}{P_s}} \quad [33]$$

$$\begin{aligned} X_m &= \text{Liquid Compressibility} \\ V_w &= \text{Well Volume (Total available volume)} \\ V_{go} &= \text{Initial Gas Kick Volume} \\ P_{go} &= \text{Initial Bubble Pressure} \\ P_s &= \text{Surface Pressure} \\ &(\text{Equation must be solved iteratively}) \end{aligned}$$

However, the equation meant to find the final surface pressure must be modified to include the initial surface pressure. The resultant equation is as follows:

$$P_{s,final} = P_{s,initial} + \frac{1}{X_m} \ln \frac{V_w - V_{go}}{V_w - \frac{P_{go}V_{go}}{P_{s,final}}} \quad [34]$$

It should be explicitly noted that the simulator used to find the pressure growth is based upon a control volume of matching cross-section to the experimental setup. The prime deliverable is a resultant pressure growth rate, accounting only for the compressibility of the test fluid; using the measured fluid compressibility before each gas kick experiment.

5.4. Total Data Set

Once each experiment was subject to the above analyses, the results were collected and combined to find the common effect of compressibility and string out on the pressure growth trend.

In the tables and graphs to follow, the liquids are referred to by number to ease organization. See Table 2 for the liquid notations and their average rheological properties.

Table 2. Test Liquid Denotations and Properties of Main Experiments

Fluid No.	Xanthan Concentration in water (% by mass)	Yield Point (lbf/100 ft ²)	Plastic Viscosity (cP)
0	0.0%	0	1
1	0.25%	7.78	2.85
2	0.50%	16.00	5.42
3	0.75%	25.46	5.29
4	1.00%	42.38	8.06

The original goal of the experiments was to find the effect of non-Newtonian fluid rheology on the rise velocity of a gas kick. Unfortunately, though a possible decreasing trend seems to appear with increasing yield stress of the liquid phase, gas entrainment also becomes an increasing issue due to the behavior of yield stress exhibiting fluids, as highlighted by Dubash and Frigaard. This increase in gas entrainment leads to small, trapped bubbles in the liquid phase to become liberated and join the larger migrating gas slug.

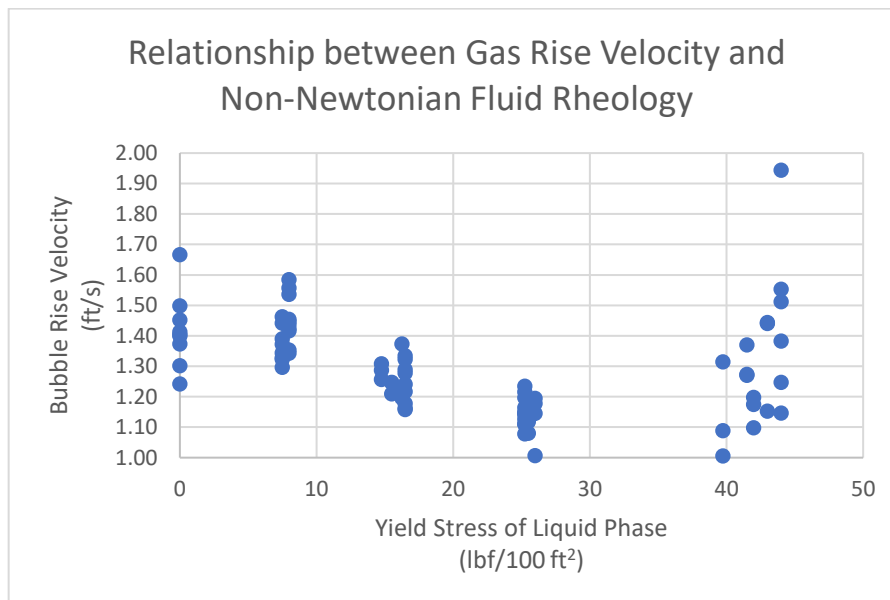


Figure 20. Gas Entrainment Precludes the Ability to Analyze the Relationship between Fluid Rheology and Bubble Rise Velocity

Accounting for compressibility is the most significant approximation that can be made from the experiments performed to zero in on the differences between expected and actual results; from there, any further deviation must be due to string out effect. As prior noted, a final surface pressure that is lower than that projected by the compressibility equation suggests string out, a final pressure that is higher than that

projected by the compressibility equation suggests the bubble has increased in mass as it traveled through the test liquid.

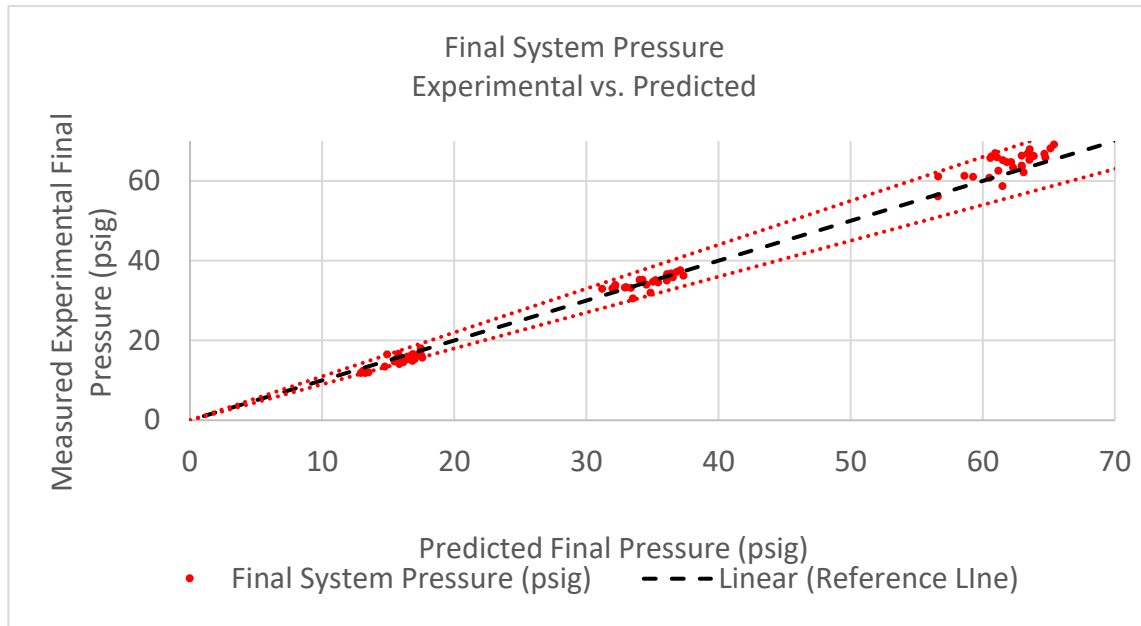


Figure 21. Measured Final System Pressure vs. Predicted Final System Pressure (+/- 10%), see Table 5 in Appendix for details

The same mechanism that depresses the final system pressure, depresses the rate at which the pressure grows. Given that the system pressure grows due to the bubble rise, if the rate at which the bubble rises is known, the pressure growth rate can be projected. In many field situations, the bubble rise velocity will be calculated by dividing the pressure rise rate by the density of the fluid, as discussed in Section 4.3 – Data Interpretation; this approach, however, assumes that the liquid phase is completely incompressible. As was found through simulating the bubble rise, when considering liquid compressibility, the pressure rise remains linear when velocity is constant. Considering the compressibility of the liquids are known, from the decompression tests performed before each test, and the velocity of the bubbles are known from the time series analysis performed, the deviation from the compressible model can be shown for each experiment.

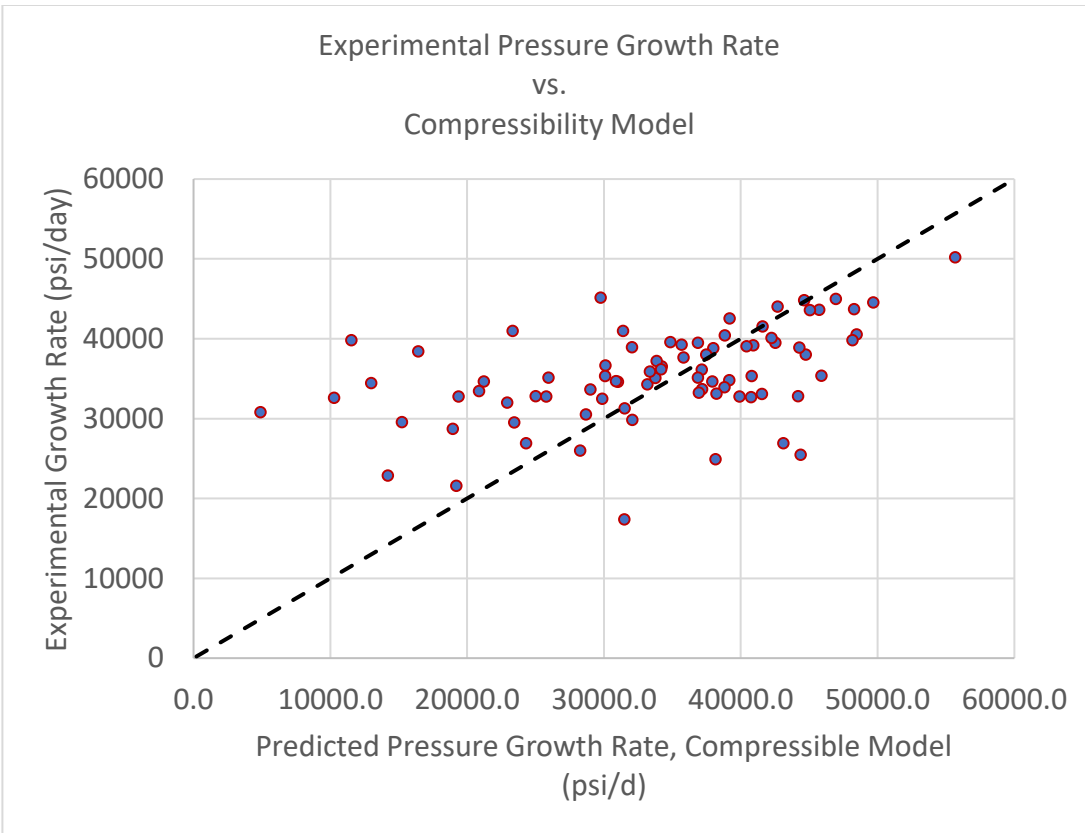


Figure 22. Experimental Pressure Growth Rates against Predicted Pressure Growth Rate Considering Bubble Rise Velocity and Liquid Compressibility. See Table 6 in Appendix for details.

As can be seen in Figure 22, the pressure growth rate deviates significantly from the predicted pressure growth rate when the rate is expected to be on the lower end (0-20,000 psi/day); the reason being the issue that was alluded to in Section 4.4 – Sources of Error, gas entrainment in the test fluid. This will be discussed in Section 5.5 – Discussion of Results. For the purposes of analyzing the mechanism of string out, one would expect that if string out is occurring, one should see a connection between the growth rate and final system pressure; the difference between the expected and measured final system pressures gives insight to how much mass the bubble has lost (or gained) as it travels through the liquid column, but the rate of pressure increase is the primary measure that is available to decision makers in a well control situation.

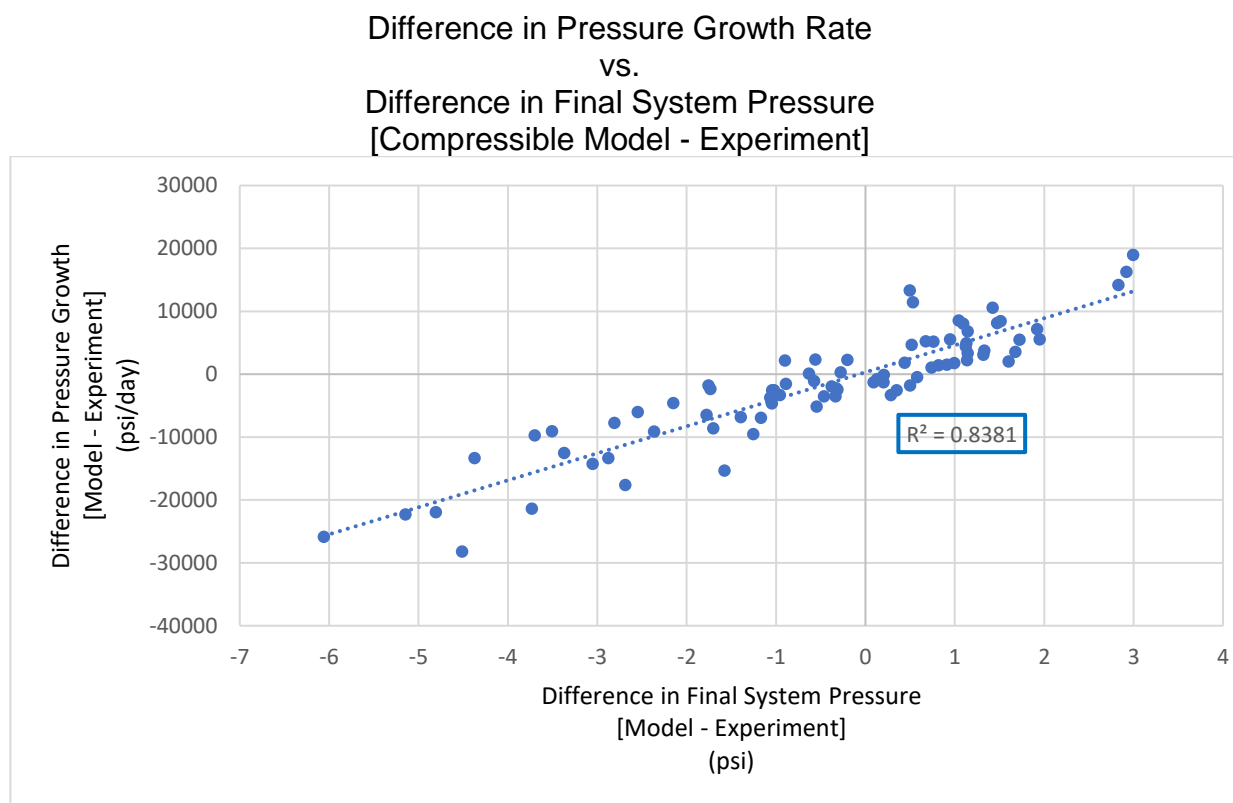


Figure 23. Difference in Pressure Growth Rate vs. Difference in Final System Pressure. If string out is occurring, it is expected that the difference in pressure growth rate should increase as the difference in final system pressure increases. See Table 6 in Appendix for details.

As can be seen in Figure 23, the deviation in pressure growth rate and final system pressure are closely correlated, as would be expected if string out is occurring. The difference in final system pressure can be considered as a proxy measurement to the mass the gas kick, or bubble in this case, is losing or gaining as it travels through the test fluid. So, it should be quite clear that as the bubble strings out along the vertical section of a well (as the difference in final system pressure increases in Figure 23), the difference between the predicted pressure growth rate and the pressure growth rate that is realized also increases; in real terms, as string out increases, the rate at which surface pressure increases will be further depressed than even that predicted by accounting for the liquid compressibility.

5.5. Estimation of Liquid Compressibility in Previously Discarded Data

During the summer of 2018, between July 20 and August 5, before compressibility and string out effects as well as gas entrainment were realized to have such a detrimental effect – relative to when the liquid phase was assumed to be incompressible – on the results, 72 gas kick experiments were performed on the same experimental setup. Because compressibility was not expected to have such a major effect – in fact compressibility was expected to have a less than 0.5% error effect on the

results, considering the pressure change that was expected within each experiment (6-7 psi) – the decompression test was not implemented until the second round of tests. Though significant compressibility was not obtained, given the results from the later experiments – described in Section 5.4 – one can estimate the final system pressure to within 10% (see Figure 21); it is conceivable to be able to estimate the compressibility of a fluid to within the same error range, given access to the other variables. In these earlier experiments, pressure, time, and volume data were all obtained, but compressibility was not.

Table 3. Fluid Denotations and Rheological Properties of Experiments from Summer 2018

Fluid No.	Xanthan Concentration	Bentonite Concentration	Yield Stress (lbf/100 ft ²)	Plastic Viscosity (cP)
1	0.50%	0.00%	1.5	1.75
2	1.00%	0.00%	45	8
3	1.50%	0.00%	74	15
4	2.00%	0.00%	78	15
5	0.50%	0.50%	19.5	7.5
6	1.00%	1.00%	43	10
7	1.50%	1.50%	97	12.5
8	2.00%	2.00%	127	19

Table 4. Summer 2018 Experiments, Average Compressibility Estimates, using Equations 32 and 33. See Table 7 in Appendix for details.

Fluid No.	Xanthan Concentration (by mass)	Bentonite Concentration (by mass)	Yield Stress (lbf/100 ft ²)	Plastic Viscosity (cP)	Average Compressibility via Eq 32 (μpsi^{-1})	Average Compressibility via Eq 33 (μpsi^{-1})
1	0.50%	0.00%	1.5	1.75	68.760	64.120
2	1.00%	0.00%	45	8	171.315	197.007
3	1.50%	0.00%	74	15	446.030	239.908
4	2.00%	0.00%	78	15	415.068	189.226
5	0.50%	0.50%	19.5	7.5	198.670	319.105
6	1.00%	1.00%	43	10	166.682	146.162
7	1.50%	1.50%	97	12.5	297.196	123.566
8	2.00%	2.00%	127	19	573.159	347.396

These results vary wildly. While the most extreme compressibility factors can be believed because of the extreme yield stresses seen in these fluids, and thus the likely extreme levels of gas entrainment in the test fluids. However, the compressibility factors below that of water are not to be believed; gas-free water was measured, via a decompression test, to result in a compressibility factor of $61.4 \times 10^{-6} \text{ psi}^{-1}$; though this is high relative to literature compressibility factors of water ($3 \times 10^{-6} \text{ psi}^{-1}$), it is likely that systematic error was created by components (valves, pressure relief valve) and an irreducible gas entrainment in the public water used consistently in all experiments have an effect on measurements.

5.6. Discussion of Results

In a real gas kick situation, a decision maker would have access to few, but important pieces of information; the pressure growth rate, liquid rheology, liquid compressibility, and kick size. In order to estimate the gas rise velocity, one would need to be able to estimate the effect of compressibility and the effect of string out; both mechanisms would have a depressive effect on pressure growth meaning the bubble is moving faster than it appears by treating the bubble as incompressible and contiguous. The experiments and subsequent analyses exhibit the effect string out can have on pressure growth rate and well surface pressure in a gas kick situation. Analysis of the older experiments shows the need for compressibility measurements on the liquid phase. The relationship and connection between pressure growth rate and final system pressure show that string out has a measurable effect that may be better analyzed with better control over the test fluid. The poor fit of experimental data to the compressible model pressure growth rate exhibits the importance of string out effects on pressure growth.

The analysis of old data shows how necessary a measure of liquid compressibility is in analyzing the data. Because there are 2 significant effects depressing pressure growth and final system pressure, the only insight into the differences between bubble rise velocity and resultant pressure growth is liquid properties. In the analysis above, it becomes obvious that assuming the pressure growth is only due to liquid compressibility, and back-calculating liquid compressibility as such leads to improper liquid compressibility factors. Because of the high gas entrainment in test fluid, excessively low compressibility factors are estimated because the gas kick is increasing in mass as it migrates up the liquid column. The same central issue arises as string out effect is related to liquid rheology.

The close correlation between difference in final top pressure transducer pressure – which, again, can be thought of as a proxy measurement for mass gained or lost by the bubble as it rises through the liquid column – and pressure growth rate (Figure 23) shows that string out effect depresses surface pressure further than that predicted by liquid compressibility and likewise depresses pressure growth rate. The final system pressure predicted by accounting for liquid compressibility brings predictions within 10%, but the pressure growth rate is much more affected by string out effects; further the difference in system pressure and the difference in pressure growth rate are closely correlated – an R^2 value of 0.837. So, if the either of these differences could be correlated to liquid properties, the other could easily be found. However,

because of poor ability to control gas entrainment in the test fluid, no such correlation can be made with the data at hand. As can be seen in Figure 23, a general, very loose correlation appears to exist of increasingly negative difference between compressible model projected final pressure and measured final pressure. However, this correlation is opposite that which would be expected; increasing yield stress should lead to more string out effect (positive difference between model and measurement), not less. What this loose correlation seems to suggest, as does a second correlation to follow in this discussion, is the test fluid held entrained gas that was added to the bubble as it migrated through the liquid column; the mass of gas adding to the primary bubble leads to higher than expected final surface pressure, and thus a 'negative' string out effect. With better control of liquid conditioning, a correlation between string out effect and liquid rheology may be attainable. The difference in measured pressure growth rates against projected pressure growth rates further reinforce the idea that gas entrainment must be controlled before a correlation between liquid rheology and string out effect can be made.

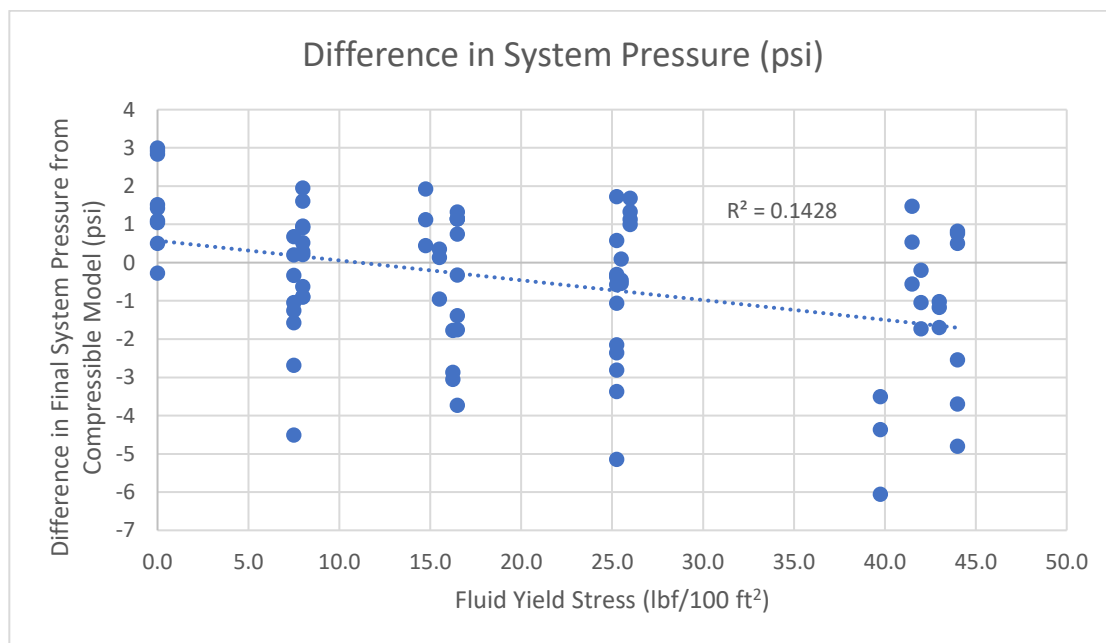


Figure 24. Possible, but Very Weak, Correlation between Liquid Yield Stress and Difference between Projected and Actual Final System Pressure

The difference between measured pressure growth rate and pressure growth rate predicted by the compressible model further reinforces the issues faced with gas entrainment in these experiments. Figure 22 shows extreme departures of measured pressure growth rates away from the expected pressure growth rates by the compressible model. Fluid 3 (0.75% Xanthan Concentration), Test #18 provides a good example of this; the projected pressure growth, assuming the test fluid is a homogenous fluid with a compressibility factor of $132.724 \times 10^{-6} \text{ psi}^{-1}$, is 10,287 psi/day but was experimentally measured at 32,596 psi/day – over 3 times greater than the compressible model would suggest. The reason for this is a failure of assumptions; the compressible model assumes that the liquid phase can be treated as a homogenous

fluid with no transfer of mass between gas and liquid phases. Unfortunately, because the high yield stress fluids entrain gas bubbles from their mixing, this assumption fails to hold true and bubble merging leads to a reverse string out effect.

The above discussion further reinforces the need for proper liquid conditioning before experiments are performed. It seems that it will be possible to estimate true bubble rise velocity when a correlation between fluid rheology and string out is developed. With proper fluid conditioning, further experimentation could provide such a correlation.

Chapter 6. Case Study

6.1. Example from Literature

At the Santa Fe Energy Bilbrey Well, a 200-barrel gas kick was taken while on a trip at 14080 ft. The well was shut in, but the gas began to migrate to surface with no way to snub in pipe to circulate the kick out of the well. Instead, the incident became a case to be shared by Consultants R.D. Grace and J.L. Shursen at a 1996 AADC/SPE Drilling Conference in New Orleans. Their intention was to assemble field level examples of gas kick rise to compare the gas kick rise velocities.

According to the information shared, the well was filled with 11.7 ppg mud at the time of kick. As the gas rose through the vertical column of fluid, its apparent rise velocity – when analyzed by the rise in surface pressure (i.e. the incompressible model) – was 400 feet per hour. But the gas reached surface as if it were migrating at 470 feet per hour. As has been shown through the experiments, it is likely for a bubble to be migrating faster than the pressure growth rate would suggest.

To analyze their findings from this example, one must make some assumptions. Because no information is included about the drilling mud other than its density, compressibility can be assumed to have a comparable value to that of water, $3 \times 10^{-6} \text{ psi}^{-1}$. The well will be considered a closed system with no further inflow or outflow. The system compressibility, due to the size of the kick, brought it close to the lower limits of the experiments performed herein; $54.6 \times 10^{-6} \text{ psi}^{-1}$ at time of kick, assuming the kick has fully displaced drilling mud at the toe of the well. Also, no temperature information was included; the system will have to be assumed to be isothermal.

Using the 2 equations put forth by Lage, Nakagawa, and Cordovil can be used to estimate the resultant pressure growth rate due to compressibility. Equation [32] leads to a direct estimate of pressure growth of 276.72 psi/hr; an apparent bubble rise velocity of 455 ft/hr. Equation [33], the final system pressure with gas kick at surface should decrease from 7806 psia at bottom hole conditions to 7564 psia; resulting in a surface pressure increase from 2715 psia to 7564 psia. The time it will take the gas kick to reach surface is estimated by dividing the stated top of gas (8422 ft) by the stated average gas rise velocity (470 ft/hr); this results in a bubble migration time of 17.9 hours. By dividing the difference in surface pressure by the gas kick travel time, an estimated pressure growth rate of 270.89 psi/hr – an apparent bubble rise velocity of 445 ft/hr.

While the compressible model shows some depression in the bubble rise estimate (~450 ft/hr versus 470 ft/hr), it does not reach the on-site estimated rise velocity of 400 ft/hr. String out effect could further depress the surface pressure growth, resulting in a lower estimate of bubble rise. Further, existence of a geothermal gradient – assuming the bottom hole is hotter than the surface location – and the fact that the system is not fully closed could have a similar effect to that of string out and compressibility. The important point is that depression of the pressure growth rate occurs at field scale level as well, though the liquid phase compressibility may be different than those that were used in the experiments.

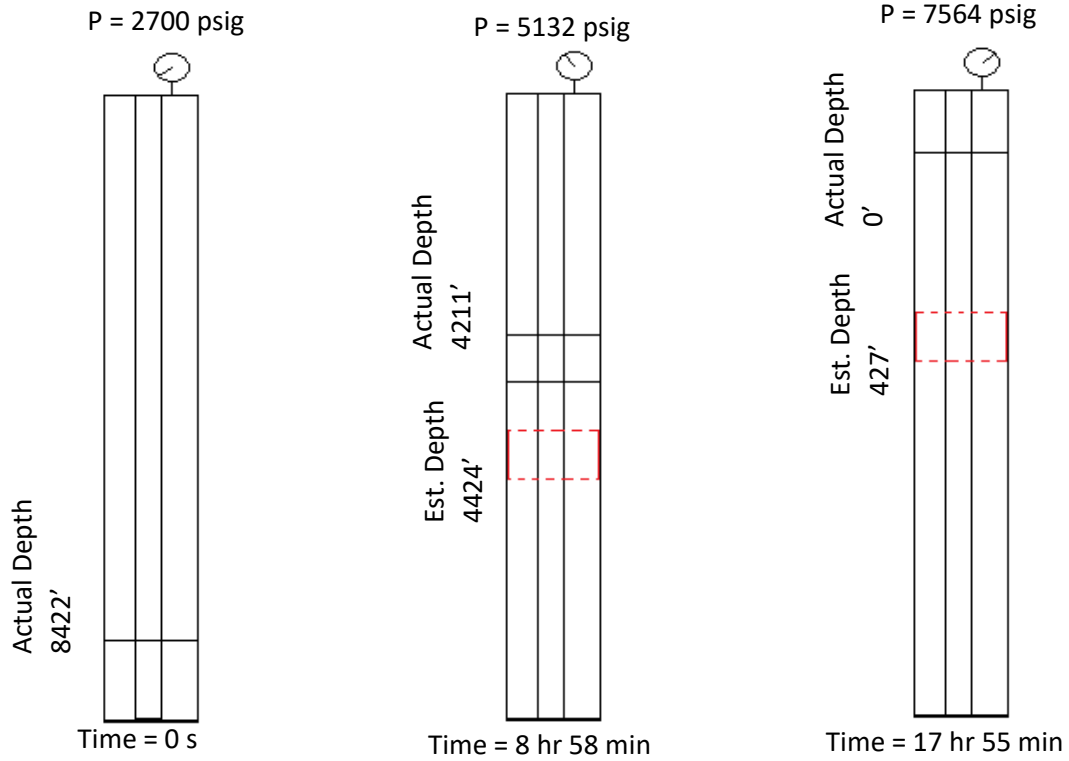


Figure 25. Visualization of Gas Kick, Actual Depth Versus Estimated Depth Over Time

6.2. Increased System Compressibility

As has been discussed throughout this manuscript, the higher the system compressibility, the more discrepancy will exist between the actual bubble rise velocity and its resultant pressure growth.

In reference to the previous example in Section 6.1, if it is assumed that the discrepancy between the true bubble rise velocity (470 ft/hr) and the estimated bubble rise velocity due to surface pressure growth (400 ft/hr) is all due to compressibility, ignoring string out effect, one finds that the liquid phase compressibility must be equal to 15.74 microsips – according to equation 32.

$$X_m = \frac{\frac{X_{go}V_{go}\rho_m g v_{slip}}{\left(\frac{dP_s}{dt}\right)} - X_{go}V_{go}}{V_m} \quad [32]$$

So, as has been described, there is an increasingly depressive effect on pressure growth as liquid phase compressibility is increased, assuming all else is kept constant.

This raises a question. For a given kick, is it possible that gas expansion reaches a point where the bubble's incremental movement upward through the liquid column can result in a negative pressure growth trend at the bottom of the well, leading to further

influx? According to equation [32], it does not appear that such a point exists; a clear asymptote exists, see Figure 25.

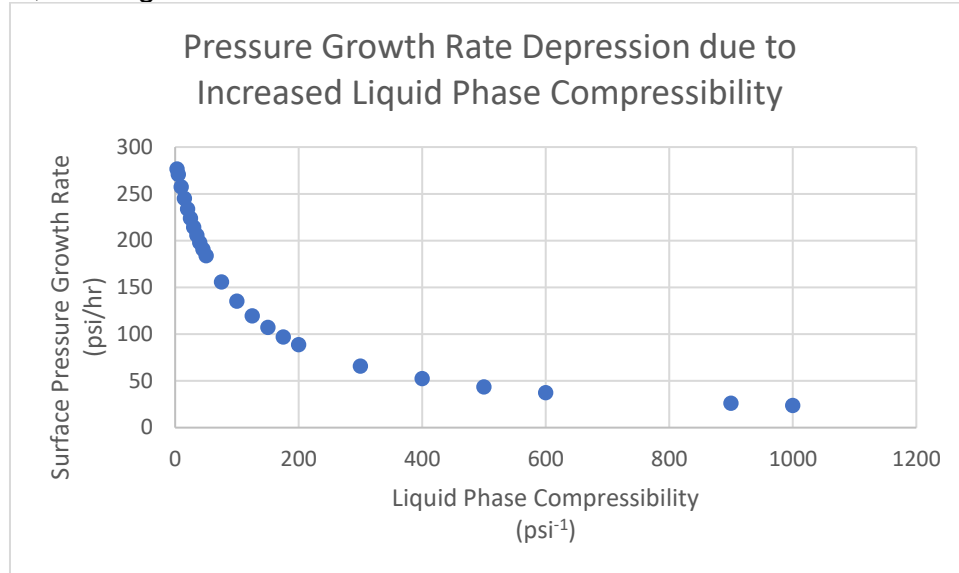


Figure 26. Relationship between Pressure Growth and Liquid Phase Compressibility for a Constant Gas Kick Size and Compressibility, according to equation 32.

Though Equation 32 suggests such a point does not exist, in running a simple simulation, similar in operation to those run for the experiments, a point of inflection indeed exists where the bubble expansion will lead to a decrease in bottom hole pressure and further influx from the formation. This suggests that for any gas kick, well geometry, and circumstance, there exists a limit to liquid phase compressibility that will acceptably allow the gas kick to migrate without allowing more influx to enter the well.

6.3. Kick Tolerance Implications

According to simulations, there exists a point in a given gas kick where rise through the liquid column allows the gas bubble to expand, leading to a decrease in bottom hole pressure, rather than the growth in pressure one would expect. Regarding kick tolerance, for a given well, a given expected gas kick rise velocity, a given mud density, there exists a limit to mud compressibility that will allow the gas kick to rise through the liquid column without allowing further influx to enter the well. This implies that for any kick that could likely occur in a drilling situation, a limit should be placed on the drilling fluid compressibility. This won't affect most system but, it could have implications for foam or low-quality foam systems.

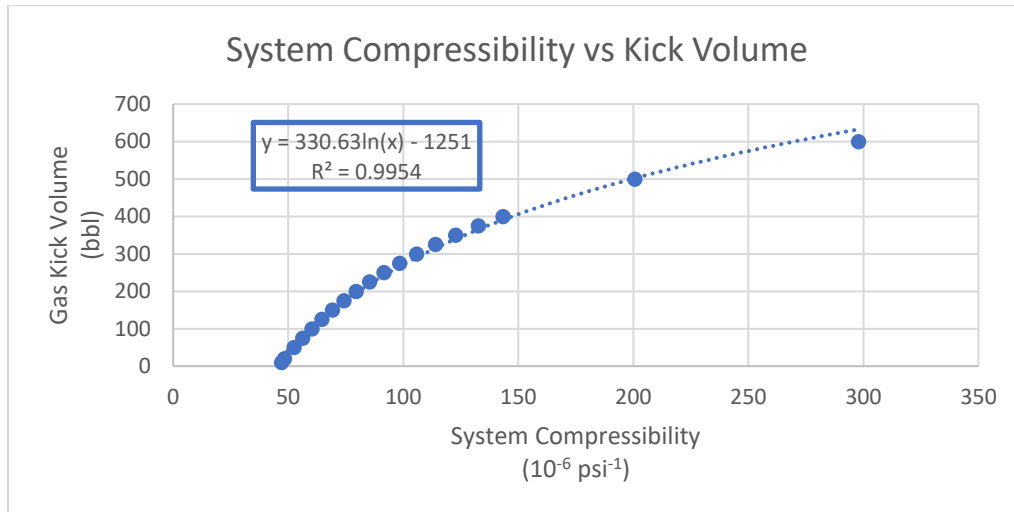


Figure 27. Balance Point between System Compressibility and Gas Kick Volume where Gas Bubble Expansion Will Allow Further Influx for a Given Gas Kick Size

Chapter 7. Conclusions

The experiments carried out in a closed system lead to the following conclusions: (1) liquid phase compressibility accounts for some – but not all – of the deviation between actual pressure trend due to gas kick rise and that expected by that suggested by the incompressible model – this is seen in both the maximum pressure to which the system rises and the rate at which the pressure increases; (2) gas kicks can lose mass at they rise through a column of liquid; (3) when the surrounding liquid phase contains entrained gas, those smaller bubbles can be liberated and join the larger bubble slug as it migrates through the liquid column – the inverse to string out effect.

Because of the significant issues encountered with liquid phase gas entrainment from mixing, further experimentation is needed to establish a correlation between string out effect and liquid rheology.

Appendix. Experimental Data

Table A.1. Difference in Final Experimental System (Surface) Pressure and Predicted Final System Pressure

Fluid No.	Test No.	Fluid Density (lbm/gal)	Fluid Compressibility (psi ⁻¹)	Initial System Pressure (psig)	Initial Bubble Pressure (psig)	Initial Bubble Volume (in ³)	Final System Pressure (psig)	Model Predicted Pressure (psig)
0	1	8.251	61.401	50.68	58.95	24.827	56.12	56.62
0	2	8.251	61.401	56.72	64.21	18.410	58.67	61.50
0	3	8.251	61.401	55.02	63.70	17.787	60.80	60.52
0	4	8.251	61.401	26.46	35.07	30.281	30.54	33.54
0	5	8.243	61.401	26.93	36.30	37.234	31.95	34.87
0	6	8.251	61.401	29.52	37.87	25.497	35.04	36.09
0	7	8.251	61.401	4.61	13.32	79.518	11.84	12.94
0	8	8.251	61.401	4.73	13.79	65.107	11.87	13.30
0	9	8.251	61.401	5.12	14.00	66.717	12.01	13.52
1	1	8.247	105.063	10.05	16.67	45.753	16.68	15.78
1	2	8.158	139.811	10.56	19.27	26.024	16.60	16.89
1	4	8.158	114.506	8.35	17.14	36.333	15.41	15.61
1	5	8.247	21.728	7.93	17.14	45.696	14.90	16.85
1	6	8.158	218.757	9.80	18.25	22.369	16.51	14.94
1	7	8.247	20.277	8.01	16.38	51.853	14.56	16.16
1	8	8.158	161.748	6.14	14.76	41.802	12.43	13.11
1	9	8.247	42.966	27.82	36.69	29.424	34.53	35.45
1	10	8.233	165.672	26.46	35.33	31.186	33.43	32.17
1	11	8.247	35.112	26.97	35.33	36.948	34.02	34.54
1	12	8.233	137.624	27.39	35.33	33.441	33.26	32.93
1	13	8.247	47.277	25.35	34.39	39.900	33.17	33.38
1	15	8.247	45.783	56.80	65.06	23.300	63.60	62.97
1	16	8.208	173.781	54.68	62.86	26.379	61.31	58.62

(table cont'd)

Fluid No.	Test No.	Fluid Density (lbm/gal)	Fluid Compressibility (psi-1)	Initial System Pressure (psig)	Initial Bubble Pressure (psig)	Initial Bubble Volume (in3)	Final System Pressure (psig)	Model Predicted Pressure (psig)
1	17	8.247	50.508	57.14	65.83	17.824	63.86	62.97
1	18	8.208	214.183	54.59	63.53	10.064	61.14	56.63
1	19	8.247	39.928	56.38	64.98	24.818	62.16	63.11
1	20	8.208	53.737	56.12	64.89	21.919	63.35	62.30
2	1	8.133	104.674	7.16	15.95	43.863	13.45	14.77
2	2	7.869	90.581	10.05	18.76	41.451	15.66	17.59
2	3	8.133	86.586	9.03	17.31	35.355	14.98	16.13
2	4	7.869	102.481	8.61	17.74	39.552	15.24	16.36
2	5	8.133	45.784	9.20	18.08	45.681	16.34	17.49
2	6	7.869	103.041	7.93	16.89	48.141	15.32	15.77
2	7	8.133	103.387	26.03	35.33	32.989	33.34	33.02
2	8	7.838	90.809	27.05	36.52	31.414	35.21	34.26
2	9	8.133	34.749	28.92	37.71	26.096	35.81	36.55
2	10	7.923	42.200	27.82	36.35	32.040	35.13	35.26
2	11	8.112	20.980	29.26	38.13	25.923	36.23	37.37
2	12	7.923	65.862	27.31	36.60	36.211	34.70	35.05
2	13	8.133	49.778	55.53	63.53	20.298	62.58	61.19
2	14	8.037	79.756	53.74	62.35	23.663	61.05	59.28
2	15	8.133	35.358	56.55	65.91	18.228	65.30	63.55
2	16	8.037	87.455	57.99	66.34	12.745	64.71	61.83
2	17	8.133	43.910	62.33	70.93	4.375	69.13	65.40
2	18	8.037	98.439	62.50	71.10	7.810	68.19	65.14
3	1	8.133	59.270	7.25	16.38	65.397	14.13	15.86
3	2	7.926	42.483	8.27	17.48	53.893	15.32	17.00

(table cont'd)

Fluid No.	Test No.	Fluid Density (lbm/gal)	Fluid Compressibility (psi-1)	Initial System Pressure (psig)	Initial Bubble Pressure (psig)	Initial Bubble Volume (in3)	Final System Pressure (psig)	Model Predicted Pressure (psig)
3	3	7.926	74.936	8.52	17.57	51.239	15.41	16.74
3	4	7.926	61.185	9.03	18.42	38.957	16.34	17.48
3	5	8.133	73.643	8.52	17.57	51.250	16.17	16.75
3	6	7.926	64.421	9.37	18.16	35.616	16.17	17.17
3	7	8.133	61.957	27.31	36.26	21.537	34.70	34.13
3	8	7.834	51.476	28.67	38.13	23.347	36.15	36.24
3	9	8.133	57.719	28.75	38.38	26.093	36.83	36.45
3	10	7.834	61.231	30.45	39.32	21.526	37.59	37.13
3	11	8.133	59.270	29.77	38.72	25.721	37.17	36.86
3	12	7.834	72.916	29.18	38.47	24.238	36.66	36.11
3	13	8.133	46.882	58.08	67.19	14.388	66.24	63.88
3	14	7.899	80.202	57.99	67.36	15.639	66.32	62.95
3	15	8.133	48.447	58.67	67.70	17.092	66.83	64.68
3	16	7.899	68.863	58.84	67.78	14.225	66.49	63.68
3	17	8.133	38.218	57.99	67.02	20.104	65.81	64.75
3	18	7.899	132.724	58.33	67.27	7.522	65.73	60.58
4	1	8.175	222.534	10.48	19.95	30.573	16.26	16.76
4	2	8.071	281.368	12.43	21.99	22.568	18.04	17.48
4	3	8.175	106.620	8.95	18.16	47.019	16.09	16.91
4	4	8.071	121.197	8.86	17.74	48.881	15.92	16.45
4	5	8.175	153.077	7.84	17.14	47.055	14.73	15.49
4	6	8.071	58.621	8.10	17.48	45.415	15.24	16.71
4	7	7.921	386.841	27.65	36.52	26.553	32.92	31.22
4	8	7.755	383.371	28.24	37.37	30.570	33.94	32.21

(table cont'd)

Fluid No.	Test No.	Fluid Density (lbm/gal)	Fluid Compressibility (psi ⁻¹)	Initial System Pressure (psig)	Initial Bubble Pressure (psig)	Initial Bubble Volume (in ³)	Final System Pressure (psig)	Model Predicted Pressure (psig)
4	9	7.921	223.924	26.71	35.75	32.346	33.00	31.98
4	10	7.755	200.237	26.29	35.84	31.487	33.09	32.05
4	11	7.921	127.837	27.56	36.69	33.819	35.21	34.04
4	12	7.755	61.401	28.75	37.79	30.444	36.32	36.12
4	13	7.514	197.913	57.99	67.27	16.770	65.90	61.09
4	14	7.778	101.940	58.50	67.87	20.903	67.94	63.57
4	15	7.514	147.297	58.25	67.02	20.298	64.71	62.16
4	16	7.778	101.940	59.10	68.55	14.930	66.92	63.41
4	17	7.514	161.799	57.99	67.44	16.378	65.22	61.52
4	18	7.778	439.558	59.18	68.80	16.607	67.00	60.94

Table A.1. Difference in Final Experimental System (Surface) Pressure and Predicted Final System Pressure

Table A.2. Difference in Pressure Growth Rate due to Bubble Rise

Fluid	Test	Fluid Density	Fluid Compressibility (psi-1)	Bubble Rise Velocity (ft/s)	Incompressible Model Pressure Growth Rate (psi/d)	Model Pressure Growth (psi/d)	Experimental Pressure Growth (psi/d)
0	1	8.251	61.401	1.4046	52066.7	38156.2	24881.1
0	2	8.251	61.401	1.2420	46038.1	31490.4	17357.5
0	3	8.251	61.401	1.4140	52412.2	31518.9	31253.0
0	4	8.251	61.401	1.4989	55560.8	44395.9	25471.9
0	5	8.243	61.401	1.6672	61743.6	43128.7	26901.7
0	6	8.251	61.401	1.3739	50928.5	41565.1	33077.1
0	7	8.251	61.401	1.4521	53826.0	48489.8	40506.3
0	8	8.251	61.401	1.3018	48254.1	45898.2	35352.7
0	9	8.251	61.401	1.4001	51898.7	48188.1	39788.5
1	1	8.247	105.063	1.4551	53913.3	45751.1	43618.2
1	2	8.158	139.811	1.5369	56328.3	39191.9	42532.5
1	4	8.158	114.506	1.3907	50968.9	42708.9	44000.0
1	5	8.247	21.728	1.5572	57697.8	55691.2	50161.5
1	6	8.158	218.757	1.3237	48515.0	29764.1	45114.2
1	7	8.247	20.277	1.3541	50172.0	46958.0	44972.2
1	8	8.158	161.748	1.4420	52851.3	49697.6	44511.0
1	9	8.247	42.966	1.4165	52482.9	45059.2	43581.3
1	10	8.233	165.672	1.3441	49716.9	31402.9	40946.6
1	11	8.247	35.112	1.3436	49782.2	48296.3	43670.6
1	12	8.233	137.624	1.4635	54131.5	35679.3	39250.0
1	13	8.247	47.277	1.4239	52757.8	44652.5	44792.5
1	15	8.247	45.783	1.4469	53610.2	41597.7	41528.4
1	16	8.208	173.781	1.2969	47822.5	23343.9	40967.7
1	17	8.247	50.508	1.4377	53269.8	38839.0	40394.8

(table cont'd)

Fluid	Test	Fluid Density	Fluid Compressibility (psi-1)	Bubble Rise Velocity (ft/s)	Incompressible Model Pressure Growth Rate (psi/d)	Model Pressure Growth (psi/d)	Experimental Pressure Growth (psi/d)
1	18	8.208	214.183	1.3723	50604.2	11551.4	39790.3
1	19	8.247	39.928	1.5850	58728.6	40811.0	35324.7
1	20	8.208	53.737	1.3283	48980.5	34870.5	39552.3
2	1	8.133	104.674	1.3347	48768.6	42543.4	39494.3
2	2	7.869	90.581	1.2574	44455.7	39919.2	32764.5
2	3	8.133	86.586	1.2781	46699.0	37924.3	34623.0
2	4	7.869	102.481	1.2880	45537.5	39164.5	34785.3
2	5	8.133	45.784	1.2899	47129.9	44760.3	37985.8
2	6	7.869	103.041	1.3082	46250.7	40932.8	39160.3
2	7	8.133	103.387	1.2412	45350.5	34233.1	36530.9
2	8	7.838	90.809	1.2465	43894.4	33857.4	37213.1
2	9	8.133	34.749	1.2171	44470.3	37169.8	36129.4
2	10	7.923	42.200	1.2103	43079.3	38007.7	38816.1
2	11	8.112	20.980	1.1786	42952.2	42257.5	40075.7
2	12	7.923	65.862	1.2481	44425.0	36887.9	39479.7
2	13	8.133	49.778	1.3228	48331.5	32056.0	38914.3
2	14	8.037	79.756	1.2248	44224.8	30127.9	36653.3
2	15	8.133	35.358	1.1621	42462.6	35822.0	37617.2
2	16	8.037	87.455	1.1958	43176.9	21240.7	34618.7
2	17	8.133	43.910	1.1582	42319.4	12988.8	34413.3
2	18	8.037	98.439	1.3738	49604.4	15246.2	29554.5
3	1	8.133	59.270	1.2157	44420.0	44302.8	38865.2
3	2	7.926	42.483	1.0067	35847.6	37180.7	33658.5
3	3	7.926	74.936	1.1785	41963.1	36957.5	33229.3

(table cont'd)

Fluid	Test	Fluid Density	Fluid Compressibility (psi-1)	Bubble Rise Velocity (ft/s)	Incompressible Model Pressure Growth Rate (psi/d)	Model Pressure Growth (psi/d)	Experimental Pressure Growth (psi/d)
3	4	7.926	61.185	1.1949	42550.0	38822.1	33917.9
3	5	8.133	73.643	1.1471	41913.6	37497.2	37986.0
3	6	7.926	64.421	1.1461	40812.4	36870.2	35107.7
3	7	8.133	61.957	1.1975	43755.3	33187.0	34284.1
3	8	7.834	51.476	1.1187	39375.4	33773.0	35089.1
3	9	8.133	57.719	1.2348	45116.1	34191.0	36140.6
3	10	7.834	61.231	1.1698	41173.2	31021.8	34592.5
3	11	8.133	59.270	1.1415	41706.7	33381.8	35880.9
3	12	7.834	72.916	1.0806	38035.8	30102.2	35293.9
3	13	8.133	46.882	1.1495	42000.0	25952.5	35102.9
3	14	7.899	80.202	1.0787	38281.4	20869.1	33419.7
3	15	8.133	48.447	1.1268	41170.3	29021.8	33639.2
3	16	7.899	68.863	1.1642	41314.7	25028.7	32796.8
3	17	8.133	38.218	1.1110	40593.5	30901.1	34654.2
3	18	7.899	132.724	1.1099	39386.8	10286.5	32596.2
4	1	8.175	222.534	1.2481	45838.6	28692.8	30522.3
4	2	8.071	281.368	1.2735	46178.8	28263.0	25983.0
4	3	8.175	106.620	1.3831	50794.8	40434.0	39033.9
4	4	8.071	121.197	1.2704	46066.8	44207.3	32798.7
4	5	8.175	153.077	1.1470	42123.9	38237.1	33108.9
4	6	8.071	58.621	1.3710	49715.6	40763.8	32655.0
4	7	7.921	386.841	1.4415	51296.9	14208.1	22849.4
4	8	7.755	383.371	1.0986	38276.8	19220.7	21579.4
4	9	7.921	223.924	1.4438	51380.0	29882.2	32454.3

(table cont'd)

Fluid	Test	Fluid Density	Fluid Compressibility (psi ⁻¹)	Bubble Rise Velocity (ft/s)	Incompressible Model Pressure Growth Rate (psi/d)	Model Pressure Growth (psi/d)	Experimental Pressure Growth (psi/d)
4	10	7.755	200.237	1.1981	41744.7	24315.6	26895.7
4	11	7.921	127.837	1.1535	41048.5	25795.1	32738.4
4	12	7.755	61.401	1.1748	40934.0	32078.8	29837.6
4	13	7.514	197.913	1.9438	65622.0	16444.4	38407.1
4	14	7.778	101.940	1.0063	35165.2	19381.3	32746.8
4	15	7.514	147.297	1.5531	52434.1	23461.1	29510.2
4	16	7.778	101.940	1.3147	45943.7	22931.9	32003.6
4	17	7.514	161.799	1.5121	51049.8	18951.9	28690.1
4	18	7.778	439.558	1.0888	38047.9	4908.5	30777.9

Table A.2. Difference in Pressure Growth Rate due to Bubble Rise; Incompressible Model, Compressible Model, and Experimental Results

Table A.3. Estimate of Liquid Phase Compressibility of Summer 2018 Experiments

Fluid	Test	Bubble Volume (in3)	Fluid Density (ppg)	dP/dt measured (psi/d)	Bubble Velocity (ft/s)	Initial System Pressure (psig)	Final System Pressure (psig)	Cf by dP/dt (psi ⁻¹)	Cf by System Pressure (psi ⁻¹)
1	1	67.054	8.3719	45664.5	1.500	3.47	12.40	263.852	46.137
1	2	36.201	8.3719	46434.9	1.472	6.28	13.16	104.019	205.248
1	3	39.080	8.3719	46291.5	1.433	6.11	13.16	96.794	201.198
1	4	30.030	8.3719	47013.2	1.409	28.72	37.90	32.661	3.020
1	5	24.682	8.3719	46422.3	1.317	29.91	38.15	13.775	26.580
1	6	29.002	8.3719	42194.2	1.334	29.31	37.81	46.320	23.078
1	7	16.455	8.3719	41061.5	1.543	57.36	63.99	37.536	37.590
1	8	16.455	8.3719	42447.8	1.355	57.87	64.84	18.112	30.848
1	9	19.746	8.3719	46067.2	1.289	57.19	66.20	5.773	3.377
2	1	64.174	8.3129	31603.8	1.023	6.45	11.46	202.165	945.024
2	2	37.435	8.3129	27772.0	1.111	4.32	10.53	296.482	326.906
2	3	38.463	8.3129	29911.8	1.515	6.62	12.82	508.623	308.007
2	4	35.172	8.3129	26441.4	1.163	26.17	32.46	203.975	157.290
2	5	29.002	8.3129	33247.0	1.168	30.25	38.07	75.366	44.444
2	6	31.264	8.3129	37195.9	1.058	31.18	39.26	16.013	37.160
2	7	43.606	8.3129	30929.5	1.819	50.05	56.68	320.065	108.459
2	8	22.626	8.3129	30525.8	0.952	54.30	62.38	21.488	18.752
2	9	28.796	8.3129	32373.6	1.022	52.60	61.87	30.244	6.367
2	10	25.505	8.3129	33666.5	1.139	54.13	62.38	38.725	17.658
3	1	34.350	8.2837	18376.2	1.481	4.32	9.42	1100.048	516.789
3	2	55.535	8.2837	24213.7	1.345	4.07	9.76	967.582	636.903
3	3	38.258	8.2837	15246.5	1.302	3.73	8.40	1366.360	725.315
3	4	21.186	8.2837	22889.3	1.335	29.99	36.45	206.953	78.657
3	5	31.881	8.2837	24845.9	0.998	29.57	36.54	133.274	89.497

(table cont'd)

Fluid	Test	Bubble Volume (in3)	Fluid Density (ppg)	dP/dt measured (psi/d)	Bubble Velocity (ft/s)	Initial System Pressure (psig)	Final System Pressure (psig)	Cf by dP/dt (psi ⁻¹)	Cf by System Pressure (psi ⁻¹)
3	6	30.030	8.2837	26546.0	0.972	28.29	36.54	94.058	30.300
3	7	18.717	8.2837	23117.5	0.781	54.39	62.29	27.596	17.736
3	8	16.661	8.2837	22797.5	1.058	57.53	64.42	66.781	31.615
3	9	17.895	8.2837	25112.6	1.027	57.36	64.33	51.619	32.358
4	1	51.833	8.2770	15215.0	0.952	3.81	9.85	1131.002	502.442
4	2	43.400	8.2770	14470.0	1.011	4.15	9.85	1122.901	492.024
4	3	53.478	8.2770	13569.1	0.685	5.00	11.38	740.667	412.278
4	4	32.087	8.2770	17181.5	0.794	26.93	33.73	205.139	104.845
4	5	24.477	8.2770	26203.4	1.383	29.91	37.90	197.006	31.253
4	6	27.356	8.2770	25313.2	1.095	30.42	37.39	138.240	75.132
4	7	20.569	8.2770	21594.9	0.754	52.52	60.59	36.082	16.831
4	8	20.157	8.2770	19329.6	0.910	56.51	63.31	84.598	40.664
4	9	21.186	8.2770	24475.1	1.102	56.43	63.91	79.976	27.565
5	1	36.201	8.3187	36346.0	1.304	7.64	13.42	176.957	347.844
5	2	70.550	8.3187	35983.0	1.845	4.49	10.44	1045.485	711.984
5	3	60.472	8.3187	39542.6	1.406	5.68	11.72	306.817	554.978
5	4	29.619	8.3187	35993.3	1.178	29.06	31.10	56.258	1029.072
5	5	28.385	8.3187	35922.7	1.190	29.31	36.71	57.339	61.730
5	6	34.555	8.3187	36568.4	1.250	28.63	36.20	82.484	67.508
5	7	22.214	8.3187	35542.0	1.157	59.23	66.71	26.005	28.679
5	8	23.243	8.3187	36268.5	1.124	58.89	65.95	19.942	39.942
5	9	23.243	8.3187	37201.8	1.127	58.72	66.20	16.743	30.210
6	1	30.442	8.3948	32127.2	1.244	4.92	10.70	218.501	330.876
6	2	44.531	8.3948	33707.9	1.301	2.71	8.91	344.567	429.497

(table cont'd)

Fluid	Test	Bubble Volume (in3)	Fluid Density (ppg)	dP/dt measured (psi/d)	Bubble Velocity (ft/s)	Initial System Pressure (psig)	Final System Pressure (psig)	Cf by dP/dt (psi ⁻¹)	Cf by System Pressure (psi ⁻¹)
6	3	42.371	8.3948	30535.4	1.411	3.39	9.68	521.038	379.391
6	4	35.378	8.3948	36918.4	1.363	28.04	35.94	120.514	56.282
6	5	16.044	8.3948	27163.0	1.303	31.86	39.43	104.109	30.707
6	6	26.328	8.3948	29527.9	0.990	29.91	37.73	58.227	43.188
6	7	20.569	8.3948	28540.0	0.975	60.25	68.33	31.687	17.063
6	8	26.122	8.3948	30257.9	0.990	59.57	68.24	32.971	10.520
6	9	22.831	8.3948	30730.0	1.261	58.04	66.20	68.523	17.933
7	1	40.315	8.4923	30111.3	1.567	2.28	8.83	681.931	341.634
7	2	52.450	8.4923	33410.8	1.619	4.32	11.55	713.725	277.083
7	3	52.861	8.4923	33321.2	1.650	3.47	10.44	776.955	337.403
7	4	31.676	8.4923	31098.5	1.430	27.44	35.52	209.140	47.482
7	5	37.024	8.4923	35957.9	1.261	27.44	35.94	109.833	35.860
7	6	38.772	8.4923	34186.6	1.110	27.78	36.03	80.705	49.391
7	7	17.278	8.4923	12314.5	1.131	56.43	61.10	240.814	103.826
7	8	21.803	8.4923	30249.9	1.053	53.37	62.72	41.514	0.963
7	9	21.494	8.4923	36663.4	1.253	48.61	56.77	40.361	20.893
7	10	17.072	8.4923	34859.5	1.655	56.60	64.33	76.985	21.122
8	1	19.540	8.6638	32521.2	1.411	56.26	63.65	75.007	33.567
8	2	21.289	8.6638	30318.7	1.352	56.94	64.25	86.679	38.156
8	3	25.505	8.6638	30223.1	1.324	55.15	62.38	101.910	49.218
8	4	38.669	8.6638	24388.0	0.927	29.91	37.56	154.995	85.952
8	5	38.669	8.6638	19506.7	1.235	29.06	34.50	480.721	273.179
8	6	34.144	8.6638	19082.5	0.856	29.87	36.32	212.687	148.439
8	7	56.975	8.6638	15918.8	1.263	5.01	10.18	1852.391	898.185

(table cont'd)

Fluid	Test	Bubble Volume (in3)	Fluid Density (ppg)	dP/dt measured (psi/d)	Bubble Velocity (ft/s)	Initial System Pressure (psig)	Final System Pressure (psig)	Cf by dP/dt (psi ⁻¹)	Cf by System Pressure (psi ⁻¹)
8	8	53.478	8.6638	14040.6	0.903	6.11	11.29	1205.437	805.803
8	9	56.152	8.6638	17926.6	0.995	5.77	11.12	988.607	794.067

Table A.3. Summer 2018 Experiments, Estimated Compressibility Factor via difference in pressure growth rate versus bubble rise velocity and difference in final system pressure. The estimated Compressibility Factors contained in the 2 rightmost columns contain widely varying and unrealistic estimated compressibility factors. Water was measured to have a compressibility of $61.4 \times 10^{-6} \text{ psi}^{-1}$ on this experimental setup.

References

1. Agarwal, V., Jana, A. K., Das, G., & Das, P. K. (2007). Taylor bubbles in liquid filled annuli: Some new observations. *Physics of Fluids*, 19(10), 108105.
2. Brown, R. A. S. (1965). The mechanics of large gas bubbles in tubes: I. Bubble velocities in stagnant liquids. *The Canadian Journal of Chemical Engineering*, 43(5), 217-223.
3. Carew, P. S., Thomas, N. H., & Johnson, A. B. (1995). A physically based correlation for the effects of power law rheology and inclination on slug bubble rise velocity. *International Journal of Multiphase Flow*, 21(6), 1091-1106.
4. Das, G., Das, P. K., Purohit, N. K., & Mitra, A. K. (1998). Rise velocity of a Taylor bubble through concentric annulus. *Chemical engineering science*, 53(5), 977-993.
5. Das, G., Purohit, N. K., Mitra, A. K., & Das, P. K. (2002). Geometry of Taylor bubbles rising through liquid-filled annuli. *AIChE journal*, 48(2), 411-416.
6. Davies, R., & Taylor, G. (1950). The Mechanics of Large Bubbles Rising through Extended Liquids and through Liquids in Tubes. *Proceedings of the Royal Society of London. Series A, Mathematical and Physical Sciences*, 200(1062), 375-390. Retrieved from <http://www.jstor.org.libezp.lib.lsu.edu/stable/98449>
7. Di Giuseppe, E., Corbi, F., Funiciello, F., Massmeyer, A., Santimano, T. N., Rosenau, M., & Davaille, A. (2015). Characterization of Carbopol® hydrogel rheology for experimental tectonics and geodynamics. *Tectonophysics*, 642, 29-45.
8. Dimakopoulos, Y., Pavlidis, M., & Tsamopoulos, J. (2013). Steady bubble rise in Herschel–Bulkley fluids and comparison of predictions via the augmented Lagrangian method with those via the Papanastasiou model. *Journal of Non-Newtonian Fluid Mechanics*, 200, 34-51.
9. Dubash, N., & Frigaard, I. (2004). Conditions for static bubbles in viscoplastic fluids. *Physics of fluids*, 16(12), 4319-4330.
10. Dubash, N., & Frigaard, I. A. (2007). Propagation and stopping of air bubbles in Carbopol solutions. *Journal of non-Newtonian fluid mechanics*, 142(1-3), 123-134.
11. Dumitrescu, D. T. (1943). Strömung an einer Luftblase im senkrechten Rohr. *ZAMM-Journal of Applied Mathematics and Mechanics/Zeitschrift für Angewandte Mathematik und Mechanik*, 23(3), 139-149.

12. Goldsmith, H. L., & Mason, S. G. (1962). The movement of single large bubbles in closed vertical tubes. *Journal of Fluid Mechanics*, 14(1), 42-58.
13. Grace, R. D., & Shursen, J. L. (1996, January 1). Field Examples of Gas Migration Rates. Society of Petroleum Engineers. doi:10.2118/35119-MS
14. Griffith, P., & Wallis, G. B. (1961). Two-phase slug flow. *Journal of Heat Transfer*, 83(3).
15. Hovland, F., & Rommetveit, R. (1992, January). Analysis of gas-rise velocities from full-scale kick experiments. In *SPE Annual Technical Conference and Exhibition*. Society of Petroleum Engineers.
16. Johnson, A. B., & White, D. B. (1993). Experimental determination of gas migration velocities with non-Newtonian fluids. *International journal of multiphase flow*, 19(6), 921-941.
17. Laird, A. D. K., & Chisholm, D. (1956). Pressure and forces along cylindrical bubbles in a vertical tube. *Industrial & Engineering Chemistry*, 48(8), 1361-1364.
18. Lage, A. C. V. M., Nakagawa, E. Y., & Cordovil, A. G. D. P. (1994, January 1). Experimental Tests for Gas Kick Migration Analysis. Society of Petroleum Engineers. doi:10.2118/26953-MS
19. Rader, D. W., Bourgoyne Jr, A., & Ward, R. H. (1975). Factors affecting bubble-rise velocity of gas kicks. *Journal of Petroleum Technology*, 27(05), 571-584.
20. Song, K. W., Kim, Y. S., & Chang, G. S. (2006). Rheology of concentrated xanthan gum solutions: Steady shear flow behavior. *Fibers and Polymers*, 7(2), 129-138.
21. Viana, F., Pardo, R., Yáñez, R., Trallero, J. L., & Joseph, D. D. (2003). Universal correlation for the rise velocity of long gas bubbles in round pipes. *Journal of Fluid Mechanics*, 494, 379-398.
22. Wallis, G. B. (1969). *One-dimensional two-phase flow*. New York, McGraw-Hill [1969].
23. Ward, R. H. (1974). *Movement of gas slugs through static liquids in large diameter annuli*. 1974.
24. White, E. T., & Beardmore, R. H. (1962). The velocity of rise of single cylindrical air bubbles through liquids contained in vertical tubes. *Chemical Engineering Science*, 17(5), 351-361.

25. Zuber, N., & Findlay, J. (1965). Average volumetric concentration in two-phase flow systems. *Journal of heat transfer*, 87(4), 453-468.
26. Zukoski, E. E. (1966). Influence of viscosity, surface tension, and inclination angle on motion of long bubbles in closed tubes. *Journal of Fluid*

VITA

Nicholas Andrew Henry, born in Houston, Texas, worked as a Completions and Well Interventions Field Supervisor for several years in Louisiana and Texas after receiving his bachelor's degree from the University of Houston. In 2014, the commodity price crashed, he turned his attention to improving his academic credentials by enrolling in the Department of Petroleum Engineering at Louisiana State University. Upon completion of his master's degree, he will begin what he hopes will be a long career with Chevron as a Deep Water Well Intervention Engineer in the Gulf of Mexico.